Available online at www.sciencedirect.com

SCIENCE DIRECT®

ELSEVIER

ISPRS Journal of Photogrammetry & Remote Sensing 59 (2005) 151–174

PHOTOGRAMMETRY & REMOTE SENSING

www.elsevier.com/locate/isprsjprs

Least squares 3D surface and curve matching

Armin Gruen, Devrim Akca*

Institute of Geodesy and Photogrammetry, Swiss Federal Institute of Technology (ETH) Zurich, ETH-Hoenggerberg, CH-8093 Zurich, Switzerland

Received 11 July 2004; received in revised form 16 February 2005; accepted 16 February 2005
Available online 29 March 2005

Abstract

The automatic co-registration of point clouds, representing 3D surfaces, is a relevant problem in 3D modeling. This multiple registration problem can be defined as a surface matching task. We treat it as least squares matching of overlapping surfaces. The surface may have been digitized/sampled point by point using a laser scanner device, a photogrammetric method or other surface measurement techniques. Our proposed method estimates the transformation parameters of one or more 3D search surfaces with respect to a 3D template surface, using the Generalized Gauss–Markoff model, minimizing the sum of squares of the Euclidean distances between the surfaces. This formulation gives the opportunity of matching arbitrarily oriented 3D surface patches. It fully considers 3D geometry. Besides the mathematical model and execution aspects we address the further extensions of the basic model. We also show how this method can be used for curve matching in 3D space and matching of curves to surfaces. Some practical examples based on the registration of close-range laser scanner and photogrammetric point clouds are presented for the demonstration of the method. This surface matching technique is a generalization of the least squares image matching concept and offers high flexibility for any kind of 3D surface correspondence problem, as well as statistical tools for the analysis of the quality of final matching results.

Keywords: Least squares 3D surface matching; 3D curve matching; Point clouds; Surface registration; Laser scanning

1. Introduction

Laser scanners can measure directly 3D coordinates of huge amounts of points in a short time period. Since the laser scanner is a line-of-sight instrument, in many cases the object has to be scanned from different viewpoints in order to completely reconstruct it. Because each scan has its own local coordinate system, all the local point clouds must be transformed into a common coordinate system. This procedure is usually referred to as registration. Actually the registration is not a problem specific to the laser scanner domain. Also

* Corresponding author. Tel.: +41 1 633 30 63; fax: +41 1 633 11 01.
E-mail address: akca@geod.baug.ethz.ch (D. Akca).

0924-2716/$ - see front matter © 2005 International Society for Photogrammetry and Remote Sensing, Inc. (ISPRS). Published by Elsevier B.V. All rights reserved.
doi:10.1016/j.isprsjprs.2005.02.006

in photogrammetry we face many similar problems. The emphasis of our work is to investigate the most general solution of the registration problem on a theoretical basis and to give practical examples for the demonstration of the method.

The following section gives an extensive literature review on previous work about 3D surface and curve matching, covering a diversity of scientific disciplines.

The proposed method is mathematically based on Least Squares Matching (LSM), which is a fundamental measurement algorithm and a powerful solution for many essential photogrammetric tasks. Section 3 briefly lists the algorithmic developments, and describes where the proposed method stands among them. Section 4 explains the basic estimation model and gives a comprehensive discussion on the implementation details, precision and reliability issues, convergence behaviour, and computational aspects. The same model can also be used for the matching of 3D space curves with each other or with a surface. This issue is addressed conceptually in Section 5. Section 6 presents some experimental results based on the registration of close-range laser scanner and photogrammetric point clouds to demonstrate the capabilities of the method. Finally, Section 7 gives the conclusions, pointing out further extensions and future works.

2. Literature review

2.1. Review of previous work on surface matching

In the past, several efforts have been made concerning the registration of 3D point clouds, especially in the Computer Vision area. One of the most popular methods is the Iterative Closest Point (ICP) algorithm developed by Besl and McKay (1992), Chen and Medioni (1992), and Zhang (1994). The original version of ICP is based on the search of pairs of nearest points in the two sets, and estimating the rigid transformation, which aligns them. Then, the rigid transformation is applied to the points of one set, and the procedure is iterated until convergence. The ICP assumes that one point set is a subset of the other. When this assumption is not valid, false matches are created which negatively influences the convergence of the ICP to the correct solution (Fusiello et al., 2002). Several variations and improvements of the ICP method have been made (Masuda and Yokoya, 1995; Bergevin et al., 1996). From a computational expense point of view it is highly time consuming due to the exhaustive search for the nearest point (Sequeira et al., 1999). In Besl and McKay (1992), and Zhang (1994) works the ICP requires every point in one surface to have a corresponding point on the other surface. An alternative approach to this search schema was proposed by Chen and Medioni (1992). They used the distance between the surfaces in the direction normal to the first surface as a registration evaluation function instead of point-to-nearest point distance. The point-to-tangent plane distance idea was originally proposed by Potmesil (1983). In Dorai et al. (1997) the method of Chen and Medioni was extended to an optimal weighted least squares framework. Zhang (1994) proposed a thresholding technique using robust statistics to limit the maximum distance between points. Masuda and Yokoya (1995) used the ICP with random sampling and least median square error measurement that is robust to a partially overlapping scene.

Okatani and Deguchi (2002) proposed the best transformation to align two range images by taking into account the measurement error properties, which is mainly dependent on both the viewing direction and the distance to the object surface. Ikemoto et al. (2003) presented a hierarchical method to align warped meshes caused by scanner calibration errors.

In the ICP algorithm and its variants main emphasis is put on the estimation of a 6-parameter rigid body transformation without uniform scale factor. There are a few reports in which higher order geometric deformations are parameterized (Feldmar and Ayache, 1996; Szeliski and Lavallee, 1996).

To tackle the exhaustive search problem of ICP Park and Subbarao (2003) gave a fast method for searching correspondences using the sensor acquisition geometry. In addition they gave an overview over the three mostly employed methods, i.e., point-to-point, point-to-(tangent) plane, and point-to-projection. Another fast implementation of the ICP using the multi-resolution and neighborhood search was given in Jost and Huegli (2003).

In Turk and Levoy (1994) a method for combining a collection of range images into a single polygonal mesh that completely describes the object was

proposed. This method first aligns the meshes with each other using a modified ICP, and stitches together adjacent meshes to form a continuous surface that correctly captures the topology of the object. Curless and Levoy (1996) proposed a volumetric method for integration of the range images. Two other volumetric approaches were given in Pulli et al. (1997), and Hilton and Illingworth (1997).

A quite different registration approach has been proposed in Johnson and Hebert (1998, 1999). Pairwise registration is accomplished using spin images, an alternative representation finding point correspondences. The final transformation is refined and verified using a modified ICP algorithm. To generate the spin image of a point in a 3D point cloud, a local basis is computed at an oriented point (3D point with surface normal) on the surface of an object represented as a polygonal surface mesh. The positions of other points with respect to the basis can then be described by two parameters. By accumulating these parameters in a 2D array, a descriptive image associated with the oriented point is created. Because the image encodes the coordinates of points on the surface of an object with respect to the local basis, it is a local description of the global shape of the object and is invariant to rigid transformations (Johnson and Hebert, 1998). In Guarnieri et al. (2003) spin images were used for the automatic detection of common areas, and initial alignment between the range image pairs.

The Iterative Closest Compatible Point (ICCP) algorithm has been proposed in order to reduce the search space of the ICP algorithm (Godin et al., 1994, 2001; Godin and Boulanger, 1995). In the ICCP algorithm, the distance minimization is performed only between the pairs of points considered compatible on the basis of their viewpoint invariant attributes (normalized color/intensity, curvature, and other attributes). In Sharp et al. (2002) a conceptually similar method called Iterative Closest Points using Invariant Features (ICPIF) has been introduced. This method chooses nearest-neighbor correspondences according to a distance metric, which is a scaled sum of the positional and feature distances. Roth (1999) proposed a method that exploits the intensity information supplied by the laser scanner device. It firstly finds the points of interest in the intensity data of each range image using an interest operator. Then, the 3D triangles, which are constructed by 2D interest points, are matched. In Stamos and Leordeanu (2003) another feature-based registration approach, which searches line and plane pairs in 3D point cloud space instead of 2D intensity image space, has been adopted. The pairwise registrations generate a graph, in which the nodes are the individual scans and the edges are the transformations between the scans. Finally, the graph algorithm registers each individual scan with respect to a central pivot scan. There can be found many other feature-based ICP approaches in the literature (Higuchi et al., 1995; Chua and Jarvis, 1996; Feldmar and Ayache, 1996; Thirion, 1996; Soucy and Ferrie, 1997; Yang and Allen, 1998; Vanden Wyngaerd et al., 1999).

In Silva et al. (2003) Genetic Algorithms (GA) in combination with hill-climbing heuristics were applied to the range image registration problem. Some comparative studies of ICP variants have been made in Rusinkiewicz and Levoy (2001) and Dalley and Flynn (2002). A highly detailed survey on the registration methods as well as recognition and 3D modeling techniques was given in Campbell and Flynn (2001).

Since most of the developed range image registration methods need an initial approximate alignment, there are some works on the issue of pre-alignment. In Murino et al. (2001) a method based on 3D skeletons was introduced. 3D skeletons are first extracted from both range images, and then matched to each other in order to find the pre-alignment. A frequency domain technique based on Fourier transformation was given in Lucchese et al. (2002) as a pre-alignment method. An automatic pre-alignment method without any prior knowledge of the relative viewpoints of the sensor or the geometry of the imaging process was given in Vanden Wyngaerd and Van Gool (2002). It matches bitangent curve pairs, which are pairs of curves that share the same tangent plane between two views. An interesting and problem-specific pre-alignment method was given in Sablatnig and Kampel (2002). They presented a method that pre-aligns the front and back views of rotationally symmetric objects, which are archeological ceramic fragments, using 3D Hough transformation. An identical voting scheme (Habib and Schenk, 1999) based on the Hough technique was used in order to find the initial approximations of the unknown 3D similarity transformation parameters between two overlapping airborne laser point clouds.

This method can solve the transformation parameters in parameter space without point correspondence. The final registration is achieved using a similar method to Chen and Medioni's (1992) point-to-tangent plane distance error minimization formula.

The well known approach for the multiple range image registration is to sequentially apply pairwise registration until all views are combined. Chen and Medioni (1992) proposed a method, which registers successive views incrementally with enough overlapping area. Each next view is registered and merged with the metaview, which is the topological union of the former pairwise registration. In Blais and Levine (1995) couples of images were incrementally registered together with a final registration between the first and last view. It is based on reversing the range finder calibration process, resulting in a set of equations, which can be used to directly compute the location of a point in a range image corresponding to an arbitrary point in three-dimensional space. Another multi image registration method based on inverse calibration, called Iterative Parametric Point (IPP), was given in Jokinen and Haggren (1995). In Bergevin et al. (1996) an algorithm, which considers the network of views as a whole and minimizes the registration errors of all views simultaneously, was introduced. This leads to a well-balanced network of views in which the registration errors are equally distributed. Pulli (1999) first aligned the scans pairwise and generated the virtual mates, which are uniformly sub-samples of the overlapping areas. The multiview alignment was performed incrementally using the virtual mates. In Dorai et al. (1998) a seamless integration method based on a weighted averaging technique for the registered multiview range data to form an unbroken surface was proposed. In Eggert et al. (1998) a force based optimization technique for simultaneous registration of multiview range images was introduced. They report that the final registration accuracy of their method typically approaches less than 1/4 of the interpoint sampling resolution of the range image.

Williams and Bennamoun (2001) proposed a new technique for the simultaneous registration of multiple point sets. The global point registration technique presented in this paper is a generalization of the well known pairwise registration method of Arun et al.'s (1987), which uses the Singular Value Decomposition (SVD) to compute the optimal registration parameters in the presence of point correspondences. This method is a closed-form solution for the 3D rigid transformation between two 3D point sets. It first reduces the unknown translation parameters, shifting all points to the center of gravity, and calculates the unknown rotation matrix using the SVD of a 3×3 matrix, and finally calculates the translation parameters. During that time two other similar methods had been developed independently based on unit quaternions (Horn, 1987; Faugeras and Hebert, 1986), but as pointed out by Horn et al. (1988) these methods were not entirely novel, since the same problem had already been treated in the Psychometry (Quantitative Psychology) literature (Schoenemann, 1966; Schoenemann and Carroll, 1970) in the name of Procrustes Analysis. An interesting note here is that the mathematical background of SVD, introduced by Eckart and Young (1936), comes from the Psychometry area. It is also known as Eckart–Young Decomposition. From a mathematical point of view a similar method to Williams and Bennamoun's (2001) proposal was given in Beinat and Crosilla (2001). They proposed the Generalized Procrustes Analysis as a solution to the multiple range image registration problem in the presence of point correspondences. More details for the Procrustes Analysis can be found in Crosilla and Beinat (2002). A further stochastic model taking into account different a priori accuracies of the tie point coordinate components was proposed by Beinat and Crosilla (2002). In fact both of the presented methods (Williams and Bennamoun, 2001; Beinat and Crosilla, 2001) use Gauss–Seidel or Jacobi type iteration techniques in order to register multiple range images simultaneously. Photogrammetric block adjustment by independent models has been proposed as another solution (Scaioni and Forlani, 2003).

Masuda (2002) proposed a method to register multiple range images using the signed distance field (SDF), which is a scalar field determined by the signed distance of an arbitrary 3D point from the object surface. In Krsek et al. (2002) an automatic hybrid registration algorithm was presented. It works in a bottom-up hierarchical mode: points-differential structures-surface. The final refinement of the estimation is carried out using Iterative Closest Reciprocal Point (ICRP) algorithm (Pajdla and Van Gool, 1995). In Castellani et al. (2002) a multiple range image

registration method was given for the 3D reconstruction of underwater environment from multiple acoustic range views acquired by a remotely operated vehicle. In addition, several reviews and comparison studies for the multiple range image registration are available in the literature (Jokinen and Haggren, 1998; Williams et al., 1999; Cunnington and Stoddart, 1999).

In Dijkman and van den Heuvel (2002) a semi-automatic registration method based on least squares fitting of the parameters of the models (cylinder and plane) was introduced. The registration is performed using the parameters of the models measured in different scans. The Global Positioning System (GPS) was also used to determine the 3D coordinates of the homologous points, which were used to merge the different scans (Balzani et al., 2002). Use of GPS allows combining all scans in a common system even if they do not have overlapping parts. To solve the point correspondence problem between two laser scanner point clouds before the 3D similarity transformation, an automatic method was proposed based on the assumption that the Z-axes of two scans are vertical (Bornaz et al., 2002). In this work retro-reflective targets, which are attached to the object surface before the scanning process, are used as common points. The idea is to search the homologous points based on two spherical coordinates (range and elevation). A similar automatic method has been given in Akca (2003) using the template shaped targets. In this work the space angles and the distances are used to solve the point correspondence problem, since they are translation and rotation invariant parameters among the different laser scanner viewpoints. The ambiguity problem, which is rare but theoretically and practically possible, is solved using consistent labeling by discrete relaxation.

This fairly exhaustive description of related research activities and achievements demonstrates the relevance of the problem. We also notice that a fully satisfying solution has still to be found, implemented and tested (see some critical comments at the beginning of Section 3).

2.2. Related work in terrain modeling

Since 3D point clouds derived by any method or device represent the object surface, the problem should be defined as a surface matching problem. In photogrammetry, the problem statement of surface patch matching and its solution method was first addressed by Gruen (1985a) as a straight extension of Least Squares Matching.

There have been some studies on the absolute orientation of stereo models using Digital Elevation Models (DEM) as control information. This work is known as DEM matching. The absolute orientation of the models using Digital Terrain Models (DTM) as control information was first proposed by Ebner and Mueller (1986), and Ebner and Strunz (1988). Afterwards, the functional model of DEM matching has been formulated by Rosenholm and Torlegard (1988). This method basically estimates the 3D similarity transformation parameters between two DEM patches, minimizing the least square differences along the Z-axes. Several applications of DEM matching have been reported (Karras and Petsa, 1993; Pilgrim, 1996; Mitchell and Chadwick, 1999; Xu and Li, 2000).

Further studies have been carried out to incorporate the DEMs into aerial block triangulation as control information (Ebner et al., 1991; Ebner and Ohlhof, 1994; Jaw, 2000). Jaw (2000) integrated the surface information into aerial triangulation by hypothesizing plane observations in object space, with a goal function that minimizes the distance along the surface normal.

Maas (2000) successfully applied a similar method to register airborne laser scanner strips, among which vertical and horizontal discrepancies generally show up due to GPS/INS accuracy problems. Another similar method has been presented for registering surfaces acquired using different techniques, in particular, laser altimetry and photogrammetry (Postolov et al., 1999).

Furthermore, techniques for 2.5D DEM surface matching have been developed, which correspond mathematically to least squares image matching. The DEM matching concept can only be applied to 2.5D surfaces, whose analytic function can be described in the explicit form as a single valued function, i.e., $z=f(x,y)$. 2.5D surfaces are of limited value in the case of generally formed objects. As a result, the DEM matching method is not fully able to solve the correspondence problem of solid 3D surfaces.

2.3. Review of previous work on curve matching

Objects in the scene can also be delineated by use of space curves instead of surfaces. In many cases the space curves carry valuable information related to the dimension and shape of the object. They can represent boundaries of regions, ridgelines, silhouettes, etc.

Matching of 2D curves is a very active research area in Computer Vision. Several algorithms, which are not explained here in detail, have been proposed in the literature. The contour matching is frequently used as another name for the same problem statement. In spite of presence of much work on curve/contour/line segment/arc matching in 2D space, only few works have been done on the problem of 3D curve matching.

As far as the current methods in Computer Vision literature are concerned, the problem has mostly been defined as that of matching of 1D feature strings, obtained from higher degree regression splines. The general attempt is to use some derived features (differential invariants, semi-differential invariants, Fourier descriptors, etc.) instead of the whole data directly (Schwartz and Sharir, 1987; Parsi et al., 1991; Kishon et al., 1991; Gueziec and Ayache, 1994; Cohen and Wang, 1994; Wang and Cohen, 1994; Pajdla and Van Gool, 1995).

Actually the ICP was proposed to solve the curve matching problem as well in both 2D and 3D space, as explained in its original publications (Besl and McKay, 1992; Zhang, 1994). Lavallee et al. (1991) presented a method that matches 3D anatomical surfaces acquired by MRI (Magnetic Resonance Imaging) or CT (Computed Tomography) to their 2D X-ray projections.

In photogrammetry, the problem statement was first touched by Gruen (1985a): "... It may even be utilized to match and analyse non-sensor data sets, such as digital height models, digital planimetric models and line map information". The LSM has been addressed as the solution, but not developed yet.

Much work has been done on the matching of line segments in image space using feature-based matching or relational matching considering the sensor geometry, auxiliary information, etc., using tree-search or relaxation techniques. Most of the work in this context focuses on automatic extraction of buildings and/or roads from aerial images.

Forkert et al. (1995) gave a method that reconstructs free-formed spatial curves represented in cubic spline form. The curve is adjusted to the bundles of rays coming from two or more images. Zalmanson and Schenk (2001) used 3D free-form curves for indirect orientation of pushbroom sensors. They addressed the advantage of using these features for providing continuous control information in object space. Although the last two references are not directly related to 3D curve matching, they give some examples on the utilization of 3D curves in photogrammetry.

An innovative work was introduced in Gruen and Li (1996) with the LSB-Snakes (Least Squares B-spline Snakes). The method of active contour models (Snakes) was formulated in a least squares approach and at the same time the technique of least squares template matching was extended by using a deformable contour instead of a rectangle as the template. This elegant method considerably improves the active contour models by using three new elements: (1) the exploitation of any a priori known geometric and photometric information to constrain the solution, (2) the simultaneous use of any number of images, and (3) the solid background of least squares estimation. Through the connection of image and object space, assuming that the interior and exterior orientation of the sensors are known, any number of images can be simultaneously accommodated and the feature can be extracted in a 2D as well as in a fully 3D mode.

3. Our proposed method

Although the registration of 3D point clouds is a very active research area in many disciplines, there is still the need for a contribution that responds favourably to the following four properties: matching of non-rigidly deformed data sets, matching of full 3D surfaces (as opposed to 2.5D), fitting of the mathematical model to the physical reality of the problem statement as well as possible, and mechanisms for internal quality control. Our proposed method meets these requirements.

The Least Squares Matching concept had been developed in parallel by Gruen (1984, 1985a), Ackermann (1984) and Pertl (1984). It has been applied to many different types of measurement and feature extraction problems due to its high level of flexibility and its powerful mathematical model: Adaptive Least Squares Image Matching (Gruen, 1984, 1985a), Geometrically Constrained Multiphoto Matching (Gruen and Baltsavias, 1988), Image Edge Matching (Gruen and Stallmann, 1991), Multiple Patch Matching with 2D images (Gruen, 1985b), Multiple Cuboid (voxel) Matching with 3D images (Maas, 1994; Maas and Gruen, 1995), Globally Enforced Least Squares Template Matching (Gruen and Agouris, 1994), Least Squares B-spline (LSB) Snakes (Gruen and Li, 1996). For a detailed survey the authors refer to Gruen (1996). If 3D point clouds derived by any device or method represent an object surface, the problem should be defined as a surface matching problem instead of the 3D point cloud matching. In particular, we treat it as Least Squares Matching of overlapping 3D surfaces, which are digitized/sampled point by point using a laser scanner device, the photogrammetric method or other surface measurement techniques. This definition allows us to find a more general solution for the problem as well as to establish a flexible mathematical model in the context of LSM.

Our mathematical model is a generalization of the Least Squares (LS) image matching, in particular the method given by Gruen (1984, 1985a). The LS image matching estimates the location of a synthetic or natural template image patch on a search image patch, modifying the search patch by an affine transformation, minimizing the sum of squares of the grey level differences between the image patches. Geometric and radiometric image deformations are simultaneously modeled via image shaping parameters and radiometric corrections. In the LS cuboid matching (Maas, 1994; Maas and Gruen, 1995) a straightforward extension to 3D voxel space working with volume data rather than image data was given. The LS surface matching conceptually stands between these two approaches.

The proposed method, Least Squares 3D Surface Matching (LS3D), matches one or more 3D search surfaces to a 3D template surface, minimizing the sum of squares of the Euclidean distances between the surfaces. This formulation gives the opportunity of matching arbitrarily oriented 3D surface patches. An observation equation is written for each element on the template surface patch, i.e. for each sampled point. The constant term of the adjustment is given by the observation vector whose elements are the Euclidean distances between the template and search surface elements. The geometric relationship between the conjugate surface patches is defined as a 7-parameter 3D similarity transformation. This parameter space can be extended or reduced, as the situation demands it. The unknown transformation parameters are treated as stochastic quantities using proper a priori weights. This extension of the mathematical model gives control over the estimation parameters. For the estimation of the parameters the Generalized Gauss–Markoff model of least squares is used. Since the estimation model provides the mechanisms for internal quality control, the localization and elimination of the gross erroneous and occluded surface subparts during the iteration is possible.

4. Least squares 3D surface matching (LS3D)

4.1. The basic estimation model

Assume that two different partial surfaces of the same object are digitized/sampled point by point, at different times (temporally) or from different viewpoints (spatially). Although the conventional sampling pattern is point based, any other type of sampling pattern is also accepted. $f(x,y,z)$ and $g(x,y,z)$ are conjugate regions of the object in the left and right surfaces respectively. In other words $f(x,y,z)$ and $g(x,y,z)$ are discrete 3D representations of the template and search surfaces. The problem statement is estimating the final location, orientation and shape of the search surface $g(x,y,z)$, which satisfies the minimum condition of Least Squares Matching with respect to the template $f(x,y,z)$. The functional model is

$$f(x,y,z) = g(x,y,z). \tag{1}$$

According to Eq. (1) each surface element on the template surface patch $f(x,y,z)$ has an exact correspondent surface element on the search surface

$g(x,y,z)$, or vice-versa, if both of the surfaces would analytically be continuous surfaces without any deterministic or stochastic discrepancies. In order to model the stochastic discrepancies, which are assumed to be random errors, and may stem from the sensor, environmental conditions or measurement method, a true error vector $e(x,y,z)$ is added as:

$$f(x,y,z) - e(x,y,z) = g(x,y,z). \tag{2}$$

Eq. (2) are observation equations, which functionally relate the observations $f(x,y,z)$ to the parameters of $g(x,y,z)$. The matching is achieved by least squares minimization of a goal function, which represents the sum of squares of the Euclidean distances between the template and the search surface elements:

$$\sum \|\vec{d}\|^2 = \min \tag{3}$$

and in Gauss form

$$[dd] = \min \tag{4}$$

where $\vec{d}$ stands for the Euclidean distance. The final location is estimated with respect to an initial position of $g(x,y,z)$, the approximation of the conjugate search surface $g^0(x,y,z)$.

To express the geometric relationship between the conjugate surface patches, a 7-parameter 3D similarity transformation is used:

$$[x \quad y \quad z]^{\mathrm{T}} = \boldsymbol{t} + m\mathbf{R}\boldsymbol{x}_0 \tag{5}$$

$$\begin{bmatrix} x \\ y \\ z \end{bmatrix} = \begin{bmatrix} t_x \\ t_y \\ t_z \end{bmatrix} + m \begin{bmatrix} r_{11} & r_{12} & r_{13} \\ r_{21} & r_{22} & r_{23} \\ r_{31} & r_{32} & r_{33} \end{bmatrix} \begin{bmatrix} x_0 \\ y_0 \\ z_0 \end{bmatrix} \tag{6}$$

where $r_{ij}=\mathbf{R}(\omega,\varphi,\kappa)$ are the elements of the orthogonal rotation matrix, $[t_x\ t_y\ t_z]^{\mathrm{T}}$ is the translation vector, and m is the uniform scale factor.

Depending on the deformation between the template and the search surfaces, any other type of 3D transformations could be used, e.g., 12-parameter affine, 24-parameter tri-linear, or 30-parameter quadratic family of transformations.

In order to perform least squares estimation, Eq. (2) must be linearized by Taylor expansion, ignoring 2nd and higher order terms.

$$\begin{aligned} f(x,y,z) - e(x,y,z) &= g^0(x,y,z) + \frac{\partial g^0(x,y,z)}{\partial x}dx \\ &\quad + \frac{\partial g^0(x,y,z)}{\partial y}dy + \frac{\partial g^0(x,y,z)}{\partial z}dz \end{aligned} \tag{7}$$

with

$$dx = \frac{\partial x}{\partial p_i}dp_i \quad , \quad dy = \frac{\partial y}{\partial p_i}dp_i \quad , \quad dz = \frac{\partial z}{\partial p_i}dp_i \tag{8}$$

where $p_i \in \{t_x,t_y,t_z,m,\omega,\varphi,\kappa\}$ is the i-th transformation parameter in Eq. (6). Differentiation of Eq. (6) gives:

$$\begin{aligned} dx &= dt_x + a_{10}dm + a_{11}d\omega + a_{12}d\varphi + a_{13}d\kappa \\ dy &= dt_y + a_{20}dm + a_{21}d\omega + a_{22}d\varphi + a_{23}d\kappa \\ dz &= dt_z + a_{30}dm + a_{31}d\omega + a_{32}d\varphi + a_{33}d\kappa \end{aligned} \tag{9}$$

where a_{ij} are the coefficient terms, whose expansions are trivial. Using the following notation

$$g_x = \frac{\partial g^0(x,y,z)}{\partial x} \quad , \quad g_y = \frac{\partial g^0(x,y,z)}{\partial y} \quad , \quad g_z = \frac{\partial g^0(x,y,z)}{\partial z} \tag{10}$$

and substituting Eq. (9), Eq. (7) results in the following:

$$\begin{aligned} -e(x,y,z) = {} & g_x dt_x + g_y dt_y + g_z dt_z \\ & + \left(g_x a_{10} + g_y a_{20} + g_z a_{30}\right)dm \\ & + \left(g_x a_{11} + g_y a_{21} + g_z a_{31}\right)d\omega \\ & + \left(g_x a_{12} + g_y a_{22} + g_z a_{32}\right)d\varphi \\ & + \left(g_x a_{13} + g_y a_{23} + g_z a_{33}\right)d\kappa \\ & - \left(f(x,y,z) - g^0(x,y,z)\right). \end{aligned} \tag{11}$$

In the context of the Gauss–Markoff model, each observation is related to a linear combination of the parameters, which are variables of a deterministic

unknown function. This function constitutes the functional model of the whole mathematical model. The terms $\{g_x, g_y, g_z\}$ are numeric 1st derivatives of this function $g(x,y,z)$.

Eq. (11) gives in matrix notation

$$-\boldsymbol{e} = \mathbf{A}\boldsymbol{x} - \boldsymbol{l} \quad , \quad \mathbf{P} \tag{12}$$

where $\mathbf{A}$ is the design matrix, $\boldsymbol{x}^{\mathrm{T}}=[dt_x\ dt_y\ dt_z\ dm\ d\omega\ d\varphi\ d\kappa]$ is the parameter vector, and $\boldsymbol{l}=f(x,y,z)-g^0(x,y,z)$ is the constant vector that consists of the Euclidean distances between the template and correspondent search surface elements. In our implementation the template surface elements are approximated by the data points. On the other hand, the search surface elements are represented by user selection of one of the two different types of piecewise surface forms (planar and bi-linear), as it will be explained in Section 4.2. In general, both surfaces (template and search) can be represented in any kind of piecewise form.

With the statistical expectation operator $\mathrm{E}\{\}$ and the assumptions

$$\boldsymbol{e} \sim \mathrm{N}\left(0, \sigma_0^2\mathbf{Q}_{ll}\right) \quad , \quad \sigma_0^2\mathbf{Q}_{ll} = \sigma_0^2\mathbf{P}_{ll}^{-1} = \mathbf{K}_{ll} = \mathrm{E}\left\{\boldsymbol{e}\boldsymbol{e}^{\mathrm{T}}\right\} \tag{13}$$

the system (12) and (13) is a Gauss–Markoff estimation model. $\mathbf{Q}_{ll}$, $\mathbf{P}=\mathbf{P}_{ll}$ and $\mathbf{K}_{ll}$ stand for a priori cofactor, weight and covariance matrices respectively.

The unknown transformation parameters are treated as stochastic quantities using proper weights. This extension gives advantages of control over the estimating parameters (Gruen, 1986). In the case of poor initial approximations for unknowns or badly distributed 3D points along the principal component axes of the surface, some of the unknowns, especially the scale factor m, may converge to a wrong solution, even if the scale factors between the surface patches are same.

We introduce the additional observation equations regarding the system parameters as

$$-\boldsymbol{e}_b = \mathbf{I}\boldsymbol{x} - \boldsymbol{l}_b \quad , \quad \mathbf{P}_b \tag{14}$$

where $\mathbf{I}$ is the identity matrix, $\boldsymbol{l}_b$ is the (fictitious) observation vector for the system parameters, and $\mathbf{P}_b$ is the associated weight coefficient matrix. The weight matrix $\mathbf{P}_b$ has to be chosen appropriately, considering a priori information of the parameters. An infinite weight value ($(\mathbf{P}_b)_{ii} \rightarrow \infty$) excludes the i-th parameter from the system assigning it as constant, whereas zero weight ($(\mathbf{P}_b)_{ii}=0$) allows the i-th parameter to vary freely assigning it as unknown parameter in the classical meaning.

The least squares solution of the joint system Eqs. (12) and (14) gives as the Generalized Gauss–Markoff model the unbiased minimum variance estimation for the parameters

$$\hat{\boldsymbol{x}} = \left(\mathbf{A}^{\mathrm{T}}\mathbf{P}\mathbf{A} + \mathbf{P}_b\right)^{-1}\left(\mathbf{A}^{\mathrm{T}}\mathbf{P}\boldsymbol{l} + \mathbf{P}_b\boldsymbol{l}_b\right) \text{ solution vector} \tag{15}$$

$$\hat{\sigma}_0^2 = \frac{\boldsymbol{v}^{\mathrm{T}}\mathbf{P}\boldsymbol{v} + \boldsymbol{v}_b^{\mathrm{T}}\mathbf{P}_b\boldsymbol{v}_b}{r} \quad \text{variance factor} \tag{16}$$

$$\boldsymbol{v} = \mathbf{A}\hat{\boldsymbol{x}} - \boldsymbol{l} \quad \text{residual vector for surface observations} \tag{17}$$

$$\boldsymbol{v}_b = \mathbf{I}\hat{\boldsymbol{x}} - \boldsymbol{l}_b \quad \text{residual vector for parameter observations} \tag{18}$$

where $\hat{}$ stands for the *Least Squares Estimator*, $r=n-u$ is the redundancy, n is the number of observations that is equivalent to the number of elements of the template surface, and u is the number of transformation parameters that is seven here. When the system converges, the solution vector converges to zero ($\hat{\boldsymbol{x}} \rightarrow 0$). Then the residuals of the surface observations $\boldsymbol{v}_i$ become the final Euclidean distances between the estimated search surface and the template surface patches.

$$\boldsymbol{v}_i = \hat{\boldsymbol{g}}(x,y,z)_i - f(x,y,z)_i \quad , \quad i = \{1, \ldots, n\}. \tag{19}$$

The function values $g(x,y,z)$ in Eq. (2) are actually stochastic quantities. This fact is neglected here to allow for the use of the Gauss–Markoff model and to avoid unnecessary complications, as typically done in LSM (Gruen, 1985a). This assumption is valid and the omissions are not significant as long as the random errors of the template and search surfaces are normally distributed and uncorrelated. In the extreme case when the random errors of both surfaces show systematic and dependency patterns, which is most probably caused by defect or imperfectness of the measurement technique or the sensor, it should be an interesting study to investigate the error behaviour using the Total Least Squares (TLS) method (Golub and Van Loan,

1980). The TLS is a relatively new adjustment method of estimating parameters in linear models that include errors in all variables (Schaffrin and Felus, 2003).

The functional model is non-linear. The solution iteratively approaches a global minimum. With the solution of linearized functional models there is always a danger to find local minima. A global minimum can only be guaranteed if the function is expanded to Taylor series at such a point where the approximate values of the parameters are close enough to their true values ($p_i^0 \cong p_i \in \mathbb{R}^u;\ i=1,\ldots,u$) in parameter space. We ensure this condition by providing of good quality initial approximations for the parameters in the first iteration:

$$p_i^0 \in \left\{ t_x^0, t_y^0, t_z^0, m^0, \omega^0 \varphi^0, \kappa^0 \right\}. \tag{20}$$

After the solution vector (15) has been solved for, the search surface is deformed to a new state using the updated set of transformation parameters, and the design matrix **A** and the constant vector $\boldsymbol{l}$ are re-evaluated. The iteration stops if each element of the alteration vector $\hat{\boldsymbol{x}}$ in Eq. (15) falls below a certain limit:

$$|dp_i| < c_i \quad , \quad dp_i \in \left\{ dt_x, dt_y, dt_z, dm, d\omega, d\varphi, d\kappa \right\} \tag{21}$$

where $i = \{1, 2, \ldots, 7\}$.

Adopting the parameters as stochastic variables allows adapting the dimension of the parameter space in a problem-specific manner. In the case of insufficient a priori information on the geometric deformation characteristics of the template and search surfaces, the adjustment could be started employing a high order transformation, e.g. 3D affine. However, this approach very often leads to an over-parameterization problem. Therefore, during the iterations an appropriate test procedure that is capable to exclude non-determinable parameters from the system should be performed. For a suitable testing strategy we refer to Gruen (1985c).

4.2. Implementation issues

The terms $\{g_x, g_y, g_z\}$ are numeric 1st derivatives of the unknown surface $g(x,y,z)$. Their calculation depends on the analytical representation of the surface elements. As a first method, let us represent the search surface elements as planar surface patches, which are constituted by fitting a plane to 3 neighboring knot points, in the *non-parametric implicit* form

$$g^0(x,y,z) = Ax + By + Cz + D = 0 \tag{22}$$

where A, B, C, and D are the parameters of the plane. The numeric 1st derivation according to the x-axis is

$$g_x = \frac{\partial g^0(x,y,z)}{\partial x} = \lim_{\Delta x \to 0} \frac{g^0(x+\Delta x, y, z) - g^0(x,y,z)}{\Delta x} \tag{23}$$

where the numerator term of the equation is simply the distance between the plane and the off-plane point $(x+\Delta x, y, z)$. Then using the point-to-plane distance formula,

$$g_x = \frac{A(x+\Delta x) + By + Cz + D}{\Delta x \sqrt{A^2 + B^2 + C^2}} = \frac{A}{\sqrt{A^2 + B^2 + C^2}} \tag{24}$$

is obtained. Similarly g_y and g_z are calculated numerically:

$$g_y = \frac{B}{\sqrt{A^2 + B^2 + C^2}} \quad , \quad g_z = \frac{C}{\sqrt{A^2 + B^2 + C^2}}. \tag{25}$$

Actually these numeric derivative values $\{g_x, g_y, g_z\}$ are x–y–z components of the local surface normal vector $\vec{n}$ at that point:

$$\begin{aligned} \vec{n} &= \begin{bmatrix} g_x \\ g_y \\ g_z \end{bmatrix} = \frac{\vec{\nabla} g^0}{\| \vec{\nabla} g^0 \|} \\ &= \frac{\left[\dfrac{\partial g^0(x,y,z)}{\partial x} \quad \dfrac{\partial g^0(x,y,z)}{\partial y} \quad \dfrac{\partial g^0(x,y,z)}{\partial z} \right]^{\mathrm{T}}}{\| \vec{\nabla} g^0 \|} \\ &= \frac{[A \quad B \quad C]^{\mathrm{T}}}{\sqrt{A^2 + B^2 + C^2}}. \end{aligned} \tag{26}$$

For the representation of the search surface elements as parametric bi-linear surface patches, a bi-linear surface is fitted to 4 neighboring knot points P_i:

$$\vec{g}^0(u,w) = [x(u,w) \quad y(u,w) \quad z(u,w)]^{\mathrm{T}} \tag{27}$$

$$\begin{aligned} \vec{g}^0(u,w) = {} & \vec{P}_1(1-u)(1-w) + \vec{P}_2(1-u)w \\ & + \vec{P}_3 u(1-w) + \vec{P}_4 uw \end{aligned} \tag{28}$$

where $u,w \in [0,1]^2$ and $\vec{g}^0(u,w), \vec{P}_i \in \mathbb{R}^3$. The vector $\vec{g}^0(u,w)$ is the position vector of any point on the bi-linear surface that is bounded by 4 knot points P_i. Again the numeric derivative terms $\{g_x, g_y, g_z\}$ are calculated from components of the local surface normal vector $\vec{n}$ on the parametric bi-linear surface patch:

$$\vec{n} = \begin{bmatrix} g_x \\ g_y \\ g_z \end{bmatrix} = \frac{\vec{\nabla} g^0}{\| \vec{\nabla} g^0 \|} = \frac{\frac{\partial \vec{g}^0(u,w)}{\partial u} \times \frac{\partial \vec{g}^0(u,w)}{\partial w}}{\| \vec{\nabla} g^0 \|} \tag{29}$$

where $\times$ stands for the vector cross product. With this approach a slightly better a posteriori σ_0-value could be obtained due to better surface modeling.

Conceptually derivative terms $\{g_x, g_y, g_z\}$ constitute a normal vector field with unit magnitude $\|\vec{n}\| = 1$ on the search surface. This vector field slides over the template surface towards the final solution, minimizing the Least Squares objective function.

4.3. Precision and reliability

The standard deviations of the estimated transformation parameters and the correlations between themselves may give useful information concerning the stability of the system and the quality of the data content (Gruen, 1985a):

$$\hat{\sigma}_p = \hat{\sigma}_0 \sqrt{q_{pp}} \quad , \quad q_{pp} \in \mathbf{Q}_{xx} = \left(\mathbf{A}^{\mathrm{T}}\mathbf{P}\mathbf{A} + \mathbf{P}_b\right)^{-1} \tag{30}$$

where $\mathbf{Q}_{xx}$ is the cofactor matrix for the estimated parameters. As pointed out in Maas (2000), the estimated standard deviations of the transformation parameters are usually too optimistic due to the stochastic properties of the search surface, which are not taken into consideration.

In order to localize and eliminate the occluded parts and the outliers a simple weighting scheme adapted from the Robust Estimation Methods is used:

$$(\mathbf{P})_{ii} = \begin{cases} 1 & \text{if} \quad |(\boldsymbol{v})_i| < K\sigma_0 \\ 0 & \text{else} \end{cases} . \tag{31}$$

In our experiments K is selected as >10, since it is aimed to suppress only the large outliers. Because of the high redundancy of a typical data arrangement, a certain amount of occlusions and/or smaller outliers do not have significant effect on the estimated parameters. As a comprehensive strategy, the data-snooping method of Baarda (1968) can be favourably used to localize the occluded or gross erroneous measurements.

4.4. Convergence of solution vector

In a standard least squares adjustment calculus, the function of the unknowns is unique, exactly known, and analytically continuous everywhere. Here the function $g(x,y,z)$ is discretized by using a finite sampling rate, which leads to slow convergence, oscillations, even divergence in some cases with respect to the standard adjustment. The convergence behaviour of the proposed method basically depends on the quality of the initial approximations and quality of the data content. For a good data configuration it usually achieves the solution after 5 or 6 iterations (Fig. 1), which is typical for LSM. To stop the

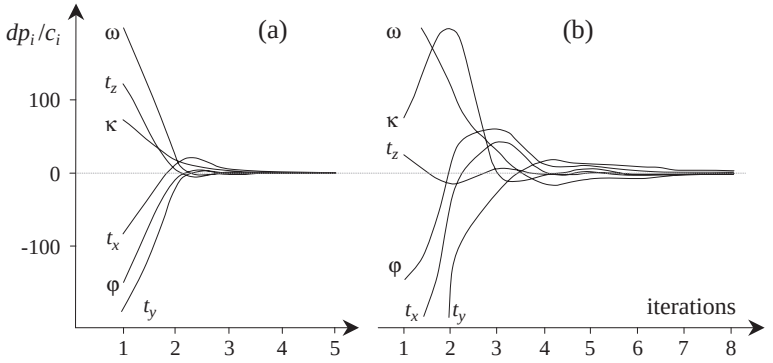

Fig. 1. Typical examples for fast convergence (a) and slow convergence (b). Note that here the scale factor m is fixed to unity.

iteration we select c_i criteria as 1.0e−5, 1.0e−4 (in given unit), and 1.0e−3 (grad) for the scale factor, translations and rotation angles respectively.

4.5. Computational aspects

The computational effort increases with the number of points in the matching process. The main portion of the computational complexity is to search the correspondent elements of the template surface patch on the search surface, whereas the adjustment part is a small system, and can quickly be solved using Cholesky decomposition followed by back-substitution. Searching the correspondence is an algorithmic problem, and needs professional software optimization techniques and programming skills, which are not within the scope of this paper.

In the case of insufficient initial approximations, the numerical derivatives $\{g_x, g_y, g_z\}$ can also be calculated on the template surface patch $f(x,y,z)$ instead of on the search surface $g(x,y,z)$ in order to speed-up the convergence. This speed-up version apparently decreases the computational effort of the design matrix **A** as well, since the derivative terms $\{f_x, f_y, f_z\}$ are calculated only once in the first iteration, and the same values are used in the following iterations. As opposed to the basic model, the number of the observation equations contributing to the design matrix **A** is here defined by the number of elements on the search surface patch $g(x,y,z)$.

Two 1st degree C^0 continuous surface representations are implemented. In the case of multi-resolution data sets, in which point densities are significantly different on the template and search surfaces, higher degree C^1 continuous composite surface representations, e.g. bi-cubic Hermit surface (Peters, 1974), should give better results, of course increasing the computational expenses.

4.6. Pros and cons of LS3D compared to some other methods

The ICP algorithm always converges monotonically to a local minimum with respect to the mean-square distance objective function (Besl and McKay, 1992). The estimation of the 6-parameters of the rigid transformation is a linear least squares solution, whereas the overall procedure is iterative. In the ICP and its variants the goal function, which minimizes the Euclidean distances between two point clouds by least squares, is achieved indirectly by estimating and applying the rigid transformations consecutively. Our mathematical model is substantially different from the ICP and its variants, since it directly formulates the goal function in a Generalized Gauss–Markoff model. The selected 3D transformation model (Eqs. 6 and 8) only relates the surfaces geometrically. The ICP needs a relatively high number of iterations (see for example Pottmann et al., 2004), while LS3D usually needs 5–8 iterations, depending also on the quality of the approximations. On the other hand, LS3D needs quite good approximations (i.e. has small convergence radius), while with ICP the requirements on the quality of the approximations are less.

In Neugebauer (1997) and Szeliski and Lavallee (1996) two gradient descent type of algorithms were given. They calculate the Euclidean distances as evaluation function value by interpolation using point-to-projection and octree spline methods respectively. They adopt the Levenberg–Marquardt method, in which diagonal elements of the normal matrix **N** are augmented by a damping matrix **D** in order to prevent numerical problems: $(\mathbf{N}+\lambda\mathbf{D})\boldsymbol{\delta}=\boldsymbol{n}$ where $\lambda>0$ is the stabilization factor that varies during the iterations. The damping matrix **D** is often chosen as an identity matrix **I** or a diagonal matrix containing the diagonal elements of the normal matrix (diag(**N**)). The Generalized Gauss–Markoff model might be seen as identical to the Levenberg–Marquardt, as the weight matrix $\mathbf{P}_b$ has a damping effect on the normal matrix. But it is a thorough statistical approach considering the a priori stochastic information (Eq. 14), and a straightforward result of the least squares formulation (Eq. 15). The Levenberg–Marquardt method is rather a numerical approach with no direct stochastical justification.

Assume that two planes are the subject of the matching process. During the solution of a standard least squares adjustment, the normal matrix becomes singular, since there is not a unique solution geometrically. This numerical reflex issues a warning to the user. On the other hand Levenberg–Marquardt will give one of the solutions out of the infinite number. Geometrically ill configured data sets are reasons for the near-singularity cases. When singularity or ill conditioning occurs, one must carefully inspect the

system and diagnose the data, instead of doing numerical manipulations.

4.7. An extension: simultaneous multi-subpatch matching

The basic estimation model can be implemented in a multi-patch mode, that is the simultaneous matching of two or more search surfaces $g_i(x,y,z)$, $i=1,\ldots,k$, to one template surface $f(x,y,z)$.

$$\begin{aligned} -\boldsymbol{e}_1 &= \mathbf{A}_1\boldsymbol{x}_1 - \boldsymbol{l}_1 \quad , \quad \mathbf{P}_1 \\ -\boldsymbol{e}_2 &= \mathbf{A}_2\boldsymbol{x}_2 - \boldsymbol{l}_2 \quad , \quad \mathbf{P}_2 \\ &\vdots \qquad\qquad \vdots \\ -\boldsymbol{e}_k &= \mathbf{A}_k\boldsymbol{x}_k - \boldsymbol{l}_k \quad , \quad \mathbf{P}_k . \end{aligned} \tag{32}$$

Since the parameter vectors $\boldsymbol{x}_1,\ldots,\boldsymbol{x}_k$ do not have any joint components, the sub-systems of Eq. (32) are orthogonal to each other. In the presence of auxiliary information those sets of equations could be connected via functional constraints, e.g. as in the Geometrically Constrained Multiphoto Matching (Gruen, 1985a; Gruen and Baltsavias, 1988) or via appropriate formulation of multiple (>2) overlap conditions.

An ordinary point cloud includes a large amount of redundant information. A straightforward way to register such two point clouds could be matching of the whole overlapping areas. This is computationally expensive. We propose multi-subpatch mode as a further extension to the basic model, which is capable of simultaneous matching of sub-surface patches, which are selected in cooperative surface areas. This leads to the observation equations

$$\begin{aligned} -\boldsymbol{e}_1 &= \mathbf{A}_1\boldsymbol{x} - \boldsymbol{l}_1 \quad , \quad \mathbf{P}_1 \\ -\boldsymbol{e}_2 &= \mathbf{A}_2\boldsymbol{x} - \boldsymbol{l}_2 \quad , \quad \mathbf{P}_2 \\ &\vdots \qquad\qquad \vdots \\ -\boldsymbol{e}_k &= \mathbf{A}_k\boldsymbol{x} - \boldsymbol{l}_k \quad , \quad \mathbf{P}_k \end{aligned} \tag{33}$$

with $i=1,\ldots,k$ subpatches.

They can be combined as in Eq. (12), since the common parameter vector $\boldsymbol{x}$ joints them to each other. The individual subpatches may not include sufficient information for the matching of whole surfaces, but together they provide a computationally effective solution, since they consist only of relevant information rather than using the full data set. One must carefully select the distribution and size of the subpatches in order to get a homogeneous quality of the transformation parameters in all directions of the 3D space. For an example of multi-subpatch matching see project Wangen-façade of Section 6.5.

5. Least squares 3D curve matching

5.1. The mathematical modelling in cubic spline form

Assume that two 3D curves of the same object are either directly measured by use of a contact measurement device, photogrammetric method, etc. or derived using any other technique. They can be matched in 3D space, since they represent the same object (Fig. 2). The curves may have been measured or extracted in a point by point fashion, but can also be in different sampling patterns. The problem statement is finding the corresponding part of the template curve $f(x,y,z)$ on the search curve $g(x,y,z)$. The analytical representation of the curves is carried out in cubic spline form, but any other piecewise representation scheme can also be considered.

In general, a parametric space curve is expressed, e.g. for the template curve, as:

$$\boldsymbol{f}(u) = [\,x(u) \quad y(u) \quad z(u)\,]^{\mathrm{T}} \tag{34}$$

where $u \in [0,1]$ and $\boldsymbol{f}(u) \in \mathbb{R}^3$ is the position vector of any point on the curve. It has three components $x(u)$,

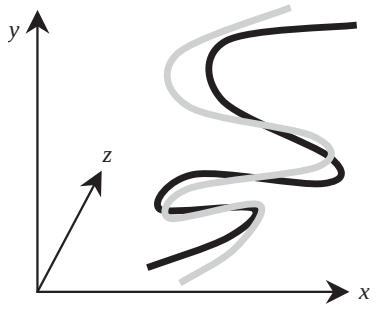

Fig. 2. Matching of free-form space curves.

$y(u)$, and $z(u)$ which may be considered as the Cartesian coordinates of the position vector (Rogers and Adams, 1976).

In the cubic spline representation

$$\boldsymbol{f}(u) = \sum_{i=1}^{4} \boldsymbol{B}_i u^{i-1} = \boldsymbol{B}_1 + \boldsymbol{B}_2 u + \boldsymbol{B}_3 u^2 + \boldsymbol{B}_4 u^3 \tag{35}$$

the coefficient vectors $\boldsymbol{B}_i \in \mathbb{R}^3$ are determined by specifying the boundary conditions for the spline segments. The expanded form shows a 4th order 3rd degree analytical definition. A cubic degree ensures the second-order continuity (C^2). This implies that the first (slope) and second (curvature) order derivatives are continuous across the joints of the composite curve. Similar expressions are also valid for the search curve:

$$\boldsymbol{g}(u) = \boldsymbol{D}_1 + \boldsymbol{D}_2 u + \boldsymbol{D}_3 u^2 + \boldsymbol{D}_4 u^3. \tag{36}$$

Using the parametric 3D space curve definition the observation equations are formulated in the same manner as explained in Section 4:

$$\boldsymbol{f}(u) - \boldsymbol{e}(u) = \boldsymbol{g}(u). \tag{37}$$

Considering the same assumptions, which have been made in the previous part, with respect to the stochastic model, the geometric relationship between the template and search curves, and the Taylor expansion, the linearized functional model evolves as:

$$\boldsymbol{f}(u) - \boldsymbol{e}(u) = \boldsymbol{g}^0(u) + \frac{\partial \boldsymbol{g}^0(u)}{\partial u} du \tag{38}$$

$$\boldsymbol{f}(u) - \boldsymbol{e}(u) = \boldsymbol{g}^0(u) + \frac{\partial \boldsymbol{g}^0(u)}{\partial u}\frac{\partial u}{\partial x} dx + \frac{\partial \boldsymbol{g}^0(u)}{\partial u}\frac{\partial u}{\partial y} dy + \frac{\partial \boldsymbol{g}^0(u)}{\partial u}\frac{\partial u}{\partial z} dz. \tag{39}$$

The relations between the Cartesian coordinate domains of the template and search curves are established via a 7-parameter 3D similarity transformation, where it is also possible to extend or reduce the parameter space of the 3D transformation upon necessity.

The differentiation of the transformation equations results in:

$$dx = \frac{\partial x}{\partial p_i} dp_i \quad , \quad dy = \frac{\partial y}{\partial p_i} dp_i \quad , \quad dz = \frac{\partial z}{\partial p_i} dp_i \tag{40}$$

where $p_i \in \{t_x, t_y, t_z, m, \omega, \varphi, \kappa\}$ is the i-th transformation parameter in Eq. (6).

The expression below

$$\frac{\partial \boldsymbol{g}^0(u)}{\partial u} = \left[\frac{\partial \boldsymbol{g}^0(u)}{\partial u}\frac{\partial u}{\partial x} \quad \frac{\partial \boldsymbol{g}^0(u)}{\partial u}\frac{\partial u}{\partial y} \quad \frac{\partial \boldsymbol{g}^0(u)}{\partial u}\frac{\partial u}{\partial z} \right]^{\mathrm{T}} = \begin{bmatrix} g_x & g_y & g_z \end{bmatrix}^{\mathrm{T}} \tag{41}$$

describes the numeric derivative terms. After further expansions, in the same manner as in the previous section, considering the parameters of the 3D transformation as fictitious observations, using an appropriate stochastic model, and with the assumptions $\mathrm{E}\{\boldsymbol{e}\} = 0$ and $\mathrm{E}\{\boldsymbol{e}\boldsymbol{e}^{\mathrm{T}}\} = \sigma_0^2 \mathbf{P}^{-1}$ the system can be formulated as a Generalized Gauss–Markoff model:

$$-\boldsymbol{e} = \mathbf{A}\boldsymbol{x} - \boldsymbol{l} \quad , \quad \mathbf{P} \tag{42}$$

$$-\boldsymbol{e}_b = \mathbf{I}\boldsymbol{x} - \boldsymbol{l}_b \quad , \quad \mathbf{P}_b. \tag{43}$$

The least squares solution of the joint system Eqs. (42) and (43) gives the unbiased minimum variance estimation for the parameters:

$$\hat{\boldsymbol{x}} = \left(\mathbf{A}^{\mathrm{T}}\mathbf{P}\mathbf{A} + \mathbf{P}_b\right)^{-1}\left(\mathbf{A}^{\mathrm{T}}\mathbf{P}\boldsymbol{l} + \mathbf{P}_b\boldsymbol{l}_b\right) \text{ solution vector} \tag{44}$$

$$\hat{\sigma}_0^2 = \frac{\boldsymbol{v}^{\mathrm{T}}\mathbf{P}\boldsymbol{v} + \boldsymbol{v}_b^{\mathrm{T}}\mathbf{P}_b\boldsymbol{v}_b}{r} \quad \text{variance factor} \tag{45}$$

$$\boldsymbol{v} = \mathbf{A}\hat{\boldsymbol{x}} - \boldsymbol{l} \quad \text{residual vector for surface observations} \tag{46}$$

$$\boldsymbol{v}_b = \mathbf{I}\hat{\boldsymbol{x}} - \boldsymbol{l}_b \quad \text{residual vector for parameter observations} \tag{47}$$

The functional model is non-linear, and the solution is iterative. The iteration stops if each element of the alteration vector $\hat{\boldsymbol{x}}$ in Eq. (44) falls below a certain limit.

Let us assume that the first three derivatives do exist and are linearly independent for a point $\boldsymbol{g}(u)$ on a parametric curve (Fig. 3). Then the first three derivatives $\boldsymbol{g}'(u)$, $\boldsymbol{g}''(u)$, and $\boldsymbol{g}'''(u)$ form a local affine coordinate system with origin $\boldsymbol{g}(u)$.

From this local affine system, one can easily obtain a local Cartesian system with origin $\boldsymbol{g}(u)$ and axes $\vec{\boldsymbol{t}},\vec{\boldsymbol{n}},\vec{\boldsymbol{b}}$ by the *Gram–Schmidt* process of orthonormalization (Farin, 1997):

$$\vec{\boldsymbol{t}} = \frac{\vec{\boldsymbol{g}}'}{\|\vec{\boldsymbol{g}}'\|} \quad , \quad \vec{\boldsymbol{b}} = \frac{\vec{\boldsymbol{g}}' \times \vec{\boldsymbol{g}}''}{\|\vec{\boldsymbol{g}}' \times \vec{\boldsymbol{g}}''\|} \quad , \quad \vec{\boldsymbol{n}} = \vec{\boldsymbol{b}} \times \vec{\boldsymbol{t}}\,. \tag{48}$$

The vectors $\vec{\boldsymbol{t}},\vec{\boldsymbol{n}},\vec{\boldsymbol{b}}$ are called tangent, (main) normal, and bi-normal vectors respectively. The frame $\vec{\boldsymbol{t}},\vec{\boldsymbol{n}},\vec{\boldsymbol{b}}$ is called moving trihedron or Frenet frame. It varies its orientation as u traces out the curve (Farin, 1997).

Considering this definition, the numeric 1st order derivative terms $\{g_x, g_y, g_z\}$ are the elements of the unit-length normal vector $\vec{\boldsymbol{n}}$ at point $\boldsymbol{g}^0(u)$.

$$[g_x \quad g_y \quad g_z]^{\mathrm{T}} = \vec{\boldsymbol{n}} \tag{49}$$

Using the proper degree and basis for curve representation, our method can handle multi-resolution and multi-sensor data sets, including multi-scale curves. It can be straightforwardly re-formulated in 2D for the matching of free-form image features.

5.2. Matching of 3D curves with a 3D surface

The same formulation allows matching of one or more 3D curve(s) with a 3D surface simultaneously (Fig. 4). The problem is finding the correspondence of a 1D geometric definition (curve) on a 2D geometric definition (surface), where both of them are parametrically represented in 3D space.

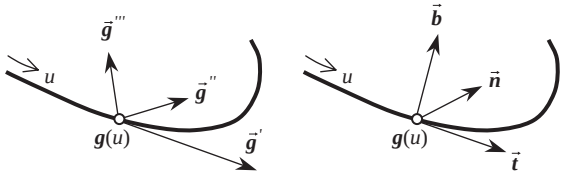

Fig. 3. Local affine system (left) and Frenet frame (right) (adapted after Farin, 1997).

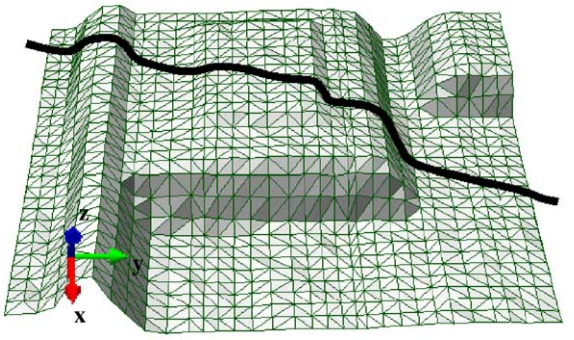

Fig. 4. Matching of a 3D space curve with a 3D surface.

6. Experimental results

Five practical examples are given to show the capabilities of the method. All experiments were carried out using own self-developed C/C+ software that runs on Microsoft Windows® OS. Processing times given in Table 1 were counted on a PC, whose configuration is Intel® P4 2.53 GHz CPU, 1 GB RAM.

In all experiments (except the example "face" in Section 6.1) the initial approximations of the unknowns were provided by interactively selecting 3 common points on both surfaces before matching. Since in all data sets there was no scale difference, the scale factor m was fixed to unity by infinite weight value ($(\mathbf{P}_b)_{ii} \rightarrow \infty$). The iteration criteria values were selected as 0.1 mm (except 0.01 mm in the example "face" in Section 6.1) for the elements of the translation vector (dt_x, dt_y, dt_z) and 10^{cc} for the rotation angles $d\omega$, $d\varphi$, $d\kappa$.

6.1. Face measurement

The first example is the registration of three surface patches, which were photogrammetrically measured 3D point clouds of a human face from multi-images (Fig. 5). For the mathematical and implementation details of this automatic surface measurement method we refer to D'Apuzzo (2002).

Left and right surface patches (Fig. 5a and c) were matched to the center surface patch (Fig. 5b) by use of LS3D. Since the data set already came in a common

Table 1
Experimental results of projects face, Wangen-relief, The Virgin Mary, Neuschwanstein

Data set	Surface mode	No. points	Iterations	Time (sec)	~point spacing (mm)	$\hat{\sigma}_0$ (mm)	$\hat{\sigma}_{tx}/\hat{\sigma}_{ty}/\hat{\sigma}_{tz}$ (mm)	$\hat{\sigma}_\omega/\hat{\sigma}_\varphi/\hat{\sigma}_\kappa$ (1.0e−02 grad)
I-L	P	2497	7	0.6	1.5	0.19	0.15/0.07/0.05	0.96/2.44/1.90
	B		7	1.3		0.19	0.15/0.07/0.05	0.96/2.42/1.91
I-R	P	3285	6	0.5	1.5	0.21	0.13/0.03/0.05	0.68/2.25/1.73
	B		6	1.4		0.21	0.13/0.03/0.05	0.69/2.26/1.75
II	P	31,520	10	6.4	10	2.45	0.22/0.16/0.07	0.24/0.27/0.48
	B		9	15.8		2.46	0.22/0.16/0.07	0.25/0.27/0.53
III	P	61,885	10	15.5	5[a]	2.12	0.07/0.11/0.08	0.44/0.15/0.50
	B		10	25.7		2.07	0.07/0.11/0.08	0.43/0.15/0.48
IV-L	P	379,121	12	294.5	9	2.20	0.01/0.02/0.02	0.06/0.04/0.03
	B		11	438.8		2.19	0.01/0.02/0.02	0.06/0.04/0.03
IV-R	P	54,469	10	17.6	6	1.71	0.04/0.02/0.04	0.06/0.05/0.06
	B		9	23.7		1.73	0.04/0.02/0.04	0.06/0.05/0.06

I: Face (L) left and (R) right, II: Wangen-relief, III: The Virgin Mary, IV: Neuschwanstein (L) left and (R) right.
P: Plane surface representation, B: bi-linear surface representation.
[a] Point density on the template surface.

coordinate system, the rotation angles (ω,φ,κ) were deteriorated by ~10[g] prior to the first iteration. Numerical results of the matching of the left surface and the right surface patches are given in parts I-L and I-R of Table 1. Relatively high standard deviations for the estimated t_x and φ (note that a high physical correlation between t_x and φ due to axes configuration occurs) are due to the narrow overlapping area along the x-axis. Nevertheless, the matching result is good. The estimated σ_0 values prove the accuracy potential of the surface measurement method, given as 0.2 mm by D'Apuzzo (2002). Since LS3D reveals the sensor noise level and accuracy potential of any kind of surface measurement method or device, it can also be used for comparison and validation studies.

6.2. Matching of a bas-relief

The second experiment refers to the matching of two overlapping 3D point clouds (Fig. 6), which represent a bas-relief on the wall of a chapel in Wangen, Germany. They were scanned using the IMAGER 5003 terrestrial laser scanner (Zoller+Fröhlich, Germany). Obtained results are given in part II of Table 1.

In the depth direction matching can be easily achieved, but in the lateral direction it is problematic due to weak surface roughness, which is around 3–4

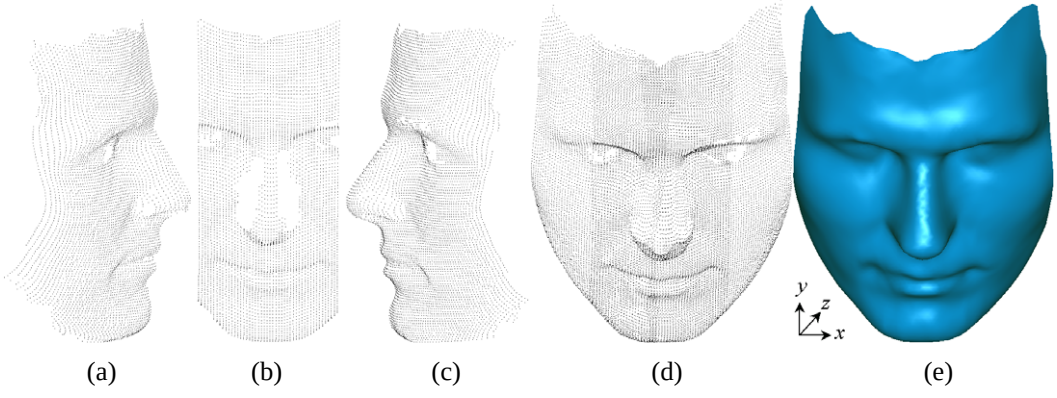

Fig. 5. Example "face". (a) Left-search surface, (b) center-template surface, (c) right-search surface, (d) obtained 3D point cloud after LS3D surface matching, (e) shaded view of the final composite surface.

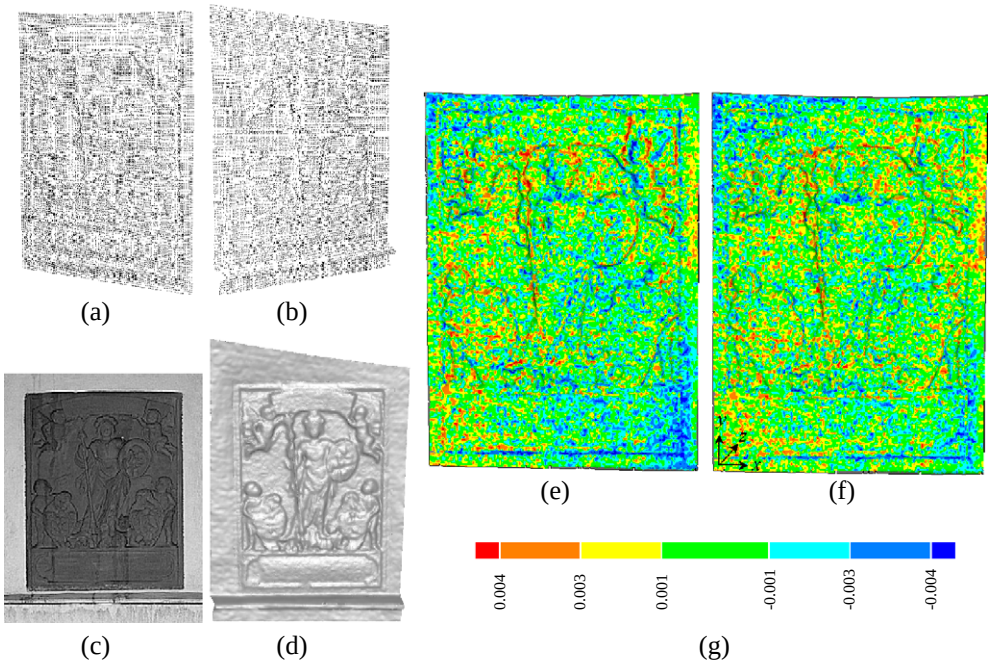

Fig. 6. Example "Wangen-relief". (a) Template surface, (b) search surface, (c) intensity image of the bas-relief, (d) final composite of the template and search surfaces after the LS3D matching method, (e) colored residuals between the fixed and transformed surfaces after the ICP method and (f) the LS3D surface matching method, (g) the residual bar in millimeter unit.

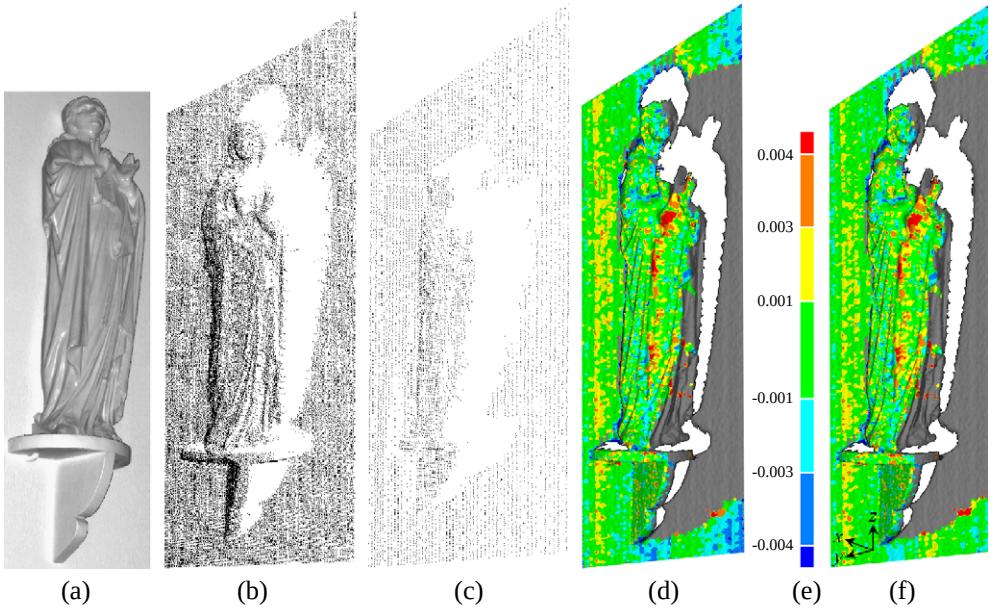

Fig. 7. Example "The Virgin Mary". (a) Intensity image of the object, (b) template surface, (c) search surface, (d) colored residuals between the fixed and transformed surfaces after the ICP method and (f) the LS3D surface matching method, (e) the residual bar in millimeter unit.

cm. In spite of this difficult data configuration the matching is successful. Relatively low theoretical precisions of the κ angle and the x, y elements of the translation vector reveal the presence of the problem. On the other hand good theoretical precision for t_z proves the excellent fit along the depth direction.

A comparison between the LS3D and ICP methods was carried out as well. The "registration" module of the Geomagic Studio v.6 (Raindrop Geomagic) was used as the ICP implementation. The fixed and floating (to be transformed) surfaces were selected as template and search surfaces, respectively. The initial approximations were given by interactively selecting 3 common points on both surfaces as identical to both procedures. Since statistical results regarding the quality of the registration were not available from the Geomagic Studio, we compared the residuals between fixed and transformed surfaces using the "3D compare" module of the same software (Fig. 6e and f). Our proposed method gives a slightly better result than the ICP considering the distribution pattern and the magnitudes of the residuals. The RMS error between the surfaces after the ICP matching is 2.55 mm, and after the LS3D matching 2.40 mm.

6.3. The Virgin Mary

This is another comparison study with respect to the ICP method. The object is a statue of the Virgin Mary on a wall of Neuschwanstein Castle in Bavaria, Germany. The IMAGER 5003 laser scanner was used to obtain the data. The search surface (Fig. 7c) was matched to the template surface (Fig. 7b). Obtained results are given in part III of Table 1. The data has an occlusion part as well as a weak configuration along the lateral direction due to the lack of sufficient geometrical information.

Again Geomagic Studio v.6 was used both for the ICP implementation and evaluation of the residuals. In this experiment both methods show a similar distribution pattern of residuals, but the LS3D method gives a slightly better RMS error (2.09 mm) than the ICP method (2.12 mm). However, the difference between the RMS errors is not significant.

6.4. Walls of Neuschwanstein Castle

The third experiment is the matching of three overlapping 3D point clouds (Fig. 8) of scans of a corridor in Neuschwanstein Castle in Bavaria, Germany. The scanning was performed by the IMAGER 5003 laser scanner. Obtained results are given as IV-L and IV-R of Table 1. The theoretical precision values of the parameters are highly optimistic. One reason for this are the stochastic properties of the search surface $g(x,y,z)$ which have not been considered as such in the estimation model.

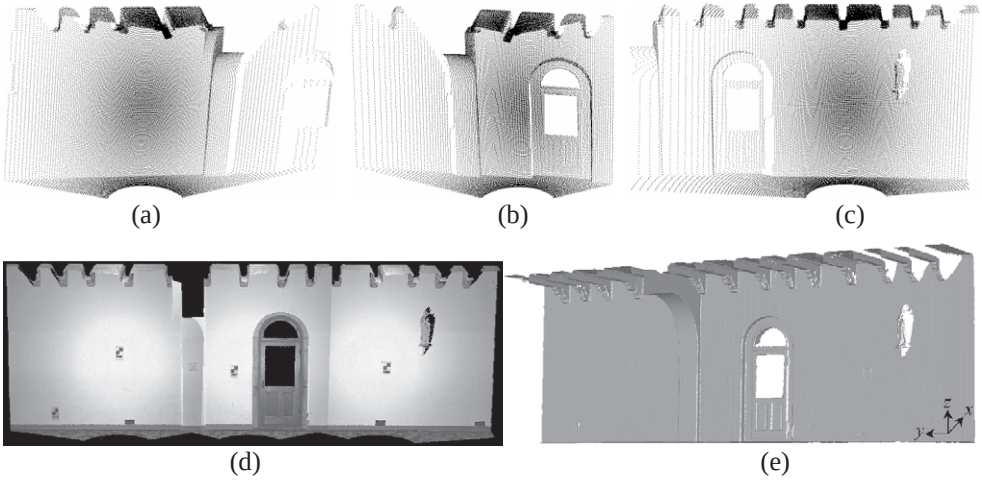

Fig. 8. Example "Neuschwanstein". (a) Left-search surface, (b) center-template surface, (c) right-search surface, (d) laser scanner derived intensities are back-projected onto the composite point cloud after LS3D matching, (e) shaded view of the final composite surface. Note that the point clouds (a), (b), and (c) are thinned out for better visualization.

Secondly, the high redundancy number with respect to the number of unknowns leads to an unrealistic precision estimation.

6.5. Façade of Wangen Chapel

The last experiment is the matching of six scans of a façade of the chapel in Wangen (Fig. 9). The scanning was performed by use of the IMAGER 5003 (Z+F) terrestrial laser scanner. Five consecutive matching processes were carried out using the simultaneous multi-subpatch approach of the LS3D. The results are given in Table 2.

The rightmost scan is matched to the template in both mono-subpatch (Fig. 9b) and multi-subpatch (Fig. 9c) modes of LS3D for comparison purposes. The visual and numerical results are given in Fig. 9d and e and in part V-1 of Table 2. The multi-patch approach gives a more homogeneous distribution of the residuals along the whole surface (see more alternating dark and light grey tones in Fig. 9e compared to 9-d), depending on the distribution of the patches, and gives slightly better theoretical precision values. As in a conventional block adjustment, it also increases the a posteriori σ_0-value, since every added patch into the system plays a quasi-

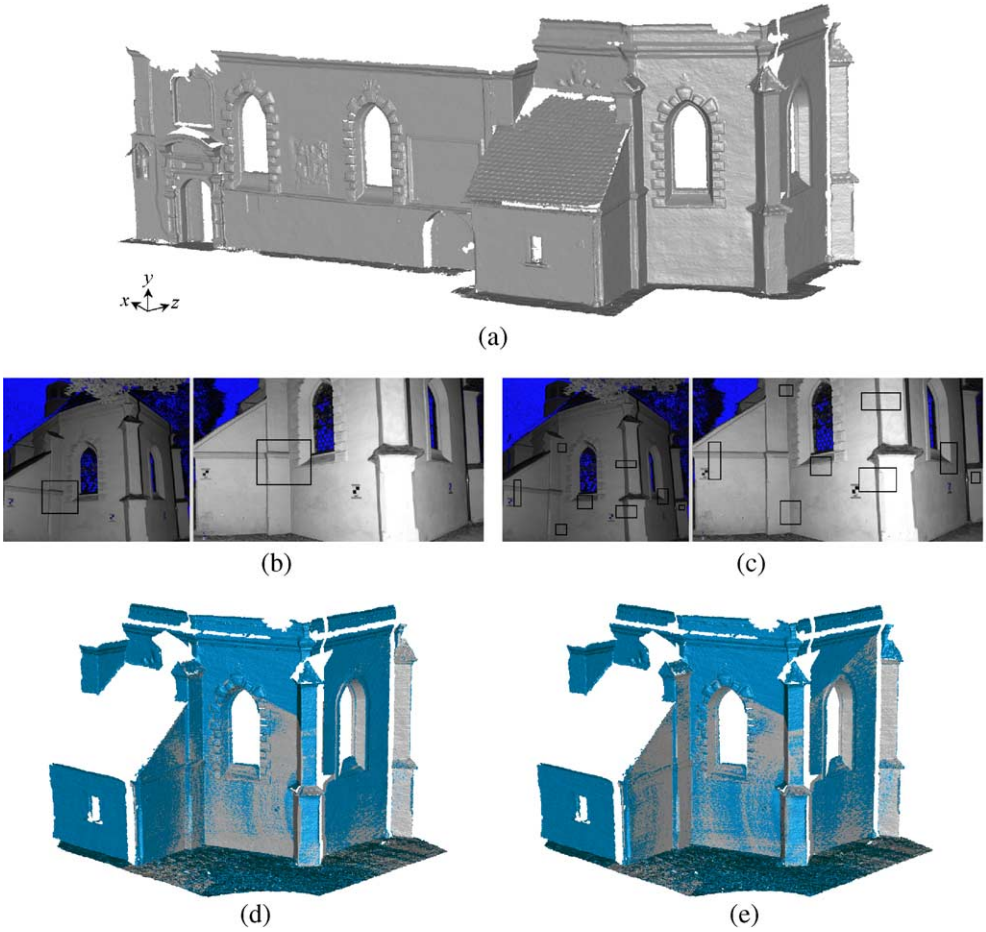

Fig. 9. Example "Wangen-façade". (a) Shaded view of the final composite surface after LS3D matching, (b) template and search (left and right) intensity images in mono-subpatch mode, (c) template and search (left and right) intensity images in multi-subpatch mode, (d) result of LS3D matching in mono-subpatch mode, (e) result of LS3D matching in multi-subpatch mode. Note that in (d) and (e) the template and search surfaces are shown in dark and light grey, respectively.

Table 2
Experimental results of multi-subpatch approach of Wangen chapel

Data set	Surface mode	No. points	Iterations	No. patches	~point spacing (mm)	$\hat{\sigma}_0$ (mm)	$\hat{\sigma}_{tx}/\hat{\sigma}_{ty}/\hat{\sigma}_{tz}$ (mm)	$\hat{\sigma}_{\omega}/\hat{\sigma}_{\varphi}/\hat{\sigma}_{\kappa}$ (1.0e−02 grad)
V-1[a]	P	12,371	5	1	15	2.66	0.13/0.62/0.58	0.51/0.42/0.45
	B		5			2.67	0.13/0.62/0.58	0.51/0.42/0.45
V-1[b]	P	12,248	6	8	15	3.42	0.06/0.33/0.15	0.24/0.12/0.24
	B		5			3.42	0.06/0.34/0.14	0.24/0.12/0.24
V-2	P	18,242	7	8	15	3.70	0.05/0.28/0.21	0.24/0.15/0.19
	B		6			3.73	0.05/0.28/0.21	0.25/0.16/0.20
V-3	P	22,753	5	5	8	3.87	0.11/0.41/0.15	0.23/0.07/0.16
	B		6			3.85	0.11/0.41/0.15	0.23/0.07/0.16
V-4	P	41,889	9	6	10	3.68	0.13/0.43/0.19	0.16/0.10/0.15
	B		7			3.70	0.14/0.47/0.19	0.16/0.10/0.16
V-5	P	30,335	10	5	10	4.53	0.28/0.75/0.33	0.21/0.14/0.21
	B		8			4.50	0.29/0.78/0.33	0.22/0.14/0.21

Part V-2,3,4, and 5 are statistical results of the sequential LS3D matching processes of scans from the right part to the left part of the façade shown in Fig. 9a.

[a] Fig. 9d mono-subpatch mode.

[b] Fig. 9e multi-subpatch mode.

control information role. In addition, the parametric bi-linear surface representation gives a slightly better convergence rate.

7. Conclusions

The proposed 3D surface matching technique is a generalization of the least squares 2D image matching concept and offers high flexibility for any kind of 3D surface correspondence problem, as well as monitoring capabilities for the analysis of the quality of the final results by means of precision and reliability criterions. Another powerful aspect of the method is its ability to handle multi-resolution, multi-temporal, multi-scale, and multi-sensor data sets. The technique can be applied to a great variety of data co-registration problems. In addition, time dependent (temporal) variations of the object surface can be inspected, tracked, and localized using the statistical analysis tools of the method.

Our method also allows the matching of space curves with each other or with a 3D surface. This gives us a hybrid formulation for feature-based matching, i.e. matching of 3D features based on the solid theory of Least Squares Matching. We also have shown how the computational effort for matching of large and many data sets can be substantially reduced by applying a subpatch matching concept. This approach uses only a selected number of small patches instead of the whole surface(s) for matching.

In this contribution, we have demonstrated the capability of this technique with the help of five different data sets. In all cases, our experiences were very positive and the procedures for internal quality control worked very well. There are several ways to refine and extend the technique.

Future work will include the verification of the theoretical expectations by more practical experimentation in order to utilize the full power of the technique. Also, we plan to use the method in a variety of different applications, including the implementation and testing of the 3D curve matching approach. Another prospect is the simultaneous matching of geometry and attribute information, e.g. temperature, intensity, color, etc., under a combined estimation model.

Acknowledgements

The authors would like to thank Dr. Nicola D'Apuzzo for providing the face surface data sets, which were measured with his software Viewtriplet GTK v0.9©. The laser scanner data sets are courtesy of Zoller+Fröhlich GmbH Elektrotechnik (Wangen, Germany). The second author is financially supported by an ETH Zurich Internal Research Grant, which is gratefully acknowledged.

References

Ackermann, F., 1984. Digital image correlation: performance and potential application in photogrammetry. Photogrammetric Record, 11 (64), 429–439.

Akca, D., 2003. Full automatic registration of laser scanner point clouds. Optical 3-D Measurement Techniques VI Zurich, September 22–25, pp. 330–337.

Arun, K.S., Huang, T.S., Blostein, S.D., 1987. Least-squares fitting of two 3D point sets. IEEE Transactions on Pattern Analysis and Machine Intelligence, 9 (5), 698–700.

Baarda, W., 1968. A Testing Procedure For Use in Geodetic Networks, vol. 2, No. 5. Netherlands Geodetic Commission, Delft. 97 p.

Balzani, M., Pellegrinelli, A., Perfetti, N., Russo, P., Uccelli, F., Tralli, S., 2002. CYRAX™ 2500 Laser scanner and GPS operational flexibility: from detailed close range surveying to urban scale surveying. CIPA WG 6 International Workshop Scanning for Cultural Heritage Recording, Corfu, September 1–2, pp. 27–32.

Beinat, A., Crosilla, F., 2001. Generalized Procrustes analysis for size and shape 3D object reconstructions. Optical 3-D Measurement Techniques V, Vienna, October 1–4, pp. 345–353.

Beinat, A., Crosilla, F., 2002. A generalized factored stochastic model for the optimal global registration of LIDAR range images. International Archives of Photogrammetry, Remote Sensing and Spatial Information Sciences, 34 (3B), 36–39.

Bergevin, R., Soucy, M., Gagnon, H., Laurendeau, D., 1996. Towards a general multi-view registration technique. IEEE Transactions on Pattern Analysis and Machine Intelligence, 18 (5), 540–547.

Besl, P.J., McKay, N.D., 1992. A method for registration of 3D shapes. IEEE Transactions on Pattern Analysis and Machine Intelligence, 14 (2), 239–256.

Blais, G., Levine, M.D., 1995. Registering multiview range data to create 3D computer objects. IEEE Transactions on Pattern Analysis and Machine Intelligence, 17 (8), 820–824.

Bornaz, L., Lingua, A., Rinaudo, F., 2002. A new software for the automatic registration of 3D digital models acquired using laser scanner devices. CIPA WG 6 International Workshop Scanning for Cultural Heritage Recording, Corfu, September 1–2, pp. 52–57.

Campbell, R.J., Flynn, P.J., 2001. A survey of free-form object representation and recognition techniques. Computer Vision and Image Understanding, 81 (2), 166–210.

Castellani, U., Fusiello, A., Murino, V., 2002. Registration of multiple acoustic range views for underwater scene reconstruction. Computer Vision and Image Understanding, 87 (1–3), 78–89.

Chen, Y., Medioni, G., 1992. Object modelling by registration of multiple range images. Image and Vision Computing, 10 (3), 145–155.

Chua, C.S., Jarvis, R., 1996. 3D free-form surface registration and object recognition. International Journal of Computer Vision, 17 (1), 77–99.

Cohen, F.S., Wang, J.Y., 1994. Part I: modeling image curves using invariant 3-D object curve models—a path to 3-D recognition and shape estimation from image contours. IEEE Transactions on Pattern Analysis and Machine Intelligence, 16 (1), 1–12.

Crosilla, F., Beinat, A., 2002. Use of Generalized Procrustes Analysis for the photogrammetric block adjustment by independent models. ISPRS Journal of Photogrammetry & Remote Sensing, 5 (63), 195–209.

Cunnington, S.J., Stoddart, A.J., 1999. N-view point set registration: a comparison. British Machine Vision Conference, Nottingham, September 13–16, pp. 234–244.

Curless, B., Levoy, M., 1996. A volumetric method for building complex models from range images. In: Rushmeier, H. (Ed.), Proceedings of SIGGRAPH'96, New Orleans, August 4–9, pp. 303–312.

Dalley, G., Flynn, P., 2002. Pair-wise range image registration: a case study in outlier classification. Computer Vision and Image Understanding, 87 (1–3), 104–115.

Dijkman, S.T., van den Heuvel, F.A., 2002. Semi automatic registration of laser scanner data. International Archives of Photogrammetry, Remote Sensing and Spatial Information Sciences, 34 (5), 12–17.

D'Apuzzo, N., 2002. Measurement and modeling of human faces from multi images. International Archives of Photogrammetry, Remote Sensing and Spatial Information Sciences, 34 (5), 241–246.

Dorai, C., Weng, J., Jain, A.K., 1997. Optimal registration of object views using range data. IEEE Transactions on Pattern Analysis and Machine Intelligence, 19 (10), 1131–1138.

Dorai, C., Wang, G., Jain, A.K., Mercer, C., 1998. Registration and integration of multiple object views for 3D model construction. IEEE Transactions on Pattern Analysis and Machine Intelligence, 20 (1), 83–89.

Ebner, H., Mueller, F., 1986. Processing of Digital Three Line Imagery using a generalized model for combined point determination. International Archives of Photogrammetry and Remote Sensing, 26 (3/1), 212–222.

Ebner, H., Strunz, G., 1988. Combined point determination using Digital Terrain Models as control information. International Archives of Photogrammetry and Remote Sensing, 27 (B11/3), 578–587.

Ebner, H., Ohlhof, T., 1994. Utilization of Ground Control Points for image orientation without point identification in image space. International Archives of Photogrammetry and Remote Sensing, 30 (3/1), 206–211.

Ebner, H., Strunz, G., Colomina, I., 1991. Block triangulation with aerial and space imagery using DTM as control information. ACSM–ASPRS Annual Convention Technical Papers, Baltimore, March 25–29, vol. 5, pp. 76–85.

Eckart, C., Young, G., 1936. The approximation of one matrix by another of lower rank. Psychometrika, 1 (3), 211–218.

Eggert, D.W., Fitzgibbon, A.W., Fisher, R.B., 1998. Simultaneous registration of multiple range views for use in reverse engineering of CAD models. Computer Vision and Image Understanding, 69 (3), 253–272.

Farin, G., 1997. Curves and Surfaces for Computer-aided Geometric Design, Fourth edition. Academic Press, USA, pp. 173–174.

Faugeras, O.D., Hebert, M., 1986. The representation, recognition, and locating of 3-D objects. The International Journal of Robotics Research, 5 (3), 27–52.

Feldmar, J., Ayache, N., 1996. Rigid, affine and locally affine registration of free-from surfaces. International Journal of Computer Vision, 18 (2), 99–119.

Forkert, G., Kerschner, M., Prinz, R., Rottensteiner, F., 1995. Reconstruction of free-formed spatial curves from digital images. International Archives of Photogrammetry and Remote Sensing, 30 (5/W1), 163–168.

Fusiello, A., Castellani, U., Ronchetti, L., Murino, V., 2002. Model acquisition by registration of multiple acoustic range views. Computer Vision-ECCV 2002. Lecture Notes in Computer Science, vol. 2351. Springer, pp. 805–819.

Godin, G., Boulager, P., 1995. Range image registration through viewpoint invariant computation of curvature. International Archives of Photogrammetyr and Remote Sensing, 30 (5/WI), 170–175.

Godin, G., Rioux, M., Baribeau, R., 1994. Three-dimensional registration using range and intensity information. Videometrics III, vol. 2350. SPIE, pp. 279–290.

Godin, G., Laurendeau, D., Bergevin, R., 2001. A method for the registration of attributed range images. IEEE International Conference on 3D Imaging and Modeling, Quebec, May 28–June 1, pp. 179–186.

Golub, G.H., Van Loan, C.F., 1980. An analysis of the total least squares problem. SIAM Journal on Numerical Analysis, 17 (6), 883–893.

Gruen, A., 1984. Adaptive least squares correlation—concept and first results. Intermediate Research Project Report to Heleva Associates, Inc. Ohio State University, Columbus, Ohio, pp. 1–13. March.

Gruen, A., 1985a. Adaptive least squares correlation: a powerful image matching technique. South African Journal of Photogrammetry, Remote Sensing and Cartography, 14 (3), 175–187.

Gruen, A., 1985b. Adaptive kleinste Quadrate Korrelation und geometrische Zusatzinformationen. Vermessung, Photogrammetrie, Kulturtechnik, 9/85, 309–312.

Gruen, A., 1985c. Data processing methods for amateur photographs. Photogrammetric Record, 11 (65), 567–579.

Gruen, A., 1986. Photogrammetrische Punktbestimmung mit der Buendelmethode. IGP ETH-Zürich, Mitteilungen, Nr. 40, pp. 1–87.

Gruen, A., 1996. Least squares matching: a fundamental measurement algorithm. In: Atkinson, K. (Ed.), Close Range Photogrammetry and Machine Vision, Whittles, pp. 217–255.

Gruen, A., Agouris, P., 1994. Linear feature extraction by least squares template matching constrained by internal shape forces. International Archives of Photogrammetry and Remote Sensing, 30 (3/1), 316–323.

Gruen, A., Baltsavias, E.P., 1988. Geometrically constrained multiphoto matching. Photogrammetric Engineering and Remote Sensing, 54 (5), 633–641.

Gruen, A., Li, H., 1996. Linear feature extraction with LSB-Snakes from multiple images. International Archives of Photogrammetry and Remote Sensing, 31 (3B), 266–272.

Gruen, A., Stallmann, D., 1991. High accuracy edge matching with an extension of the MPGC matching algorithm. International Conference on Industrial Vision Metrology, Winnipeg, July 11–12, vol. 1526. SPIE, pp. 42–55.

Guarnieri, A., Guidi, G., Tucci, G., Vettore, A., 2003. Towards automatic modeling for cultural heritage applications. International Archives of Photogrammetry, Remote Sensing and Spatial Information Sciences, 34 (5/W12), 176–181.

Gueziec, A., Ayache, N., 1994. Smoothing and matching of 3-D space curves. International Journal of Computer Vision, 12 (1), 79–104.

Habib, A., Schenk, T., 1999. A new approach for matching surfaces from laser scanners and optical scanners. International Archives of Photogrammetry and Remote Sensing, 32 (3/W14), 55–61.

Higuchi, K., Hebert, M., Ikeuchi, K., 1995. Building 3D models from unregistered range images. Graphical Models and Image Processing, 57 (4), 315–333.

Hilton, A., Illingworth, J., 1997. Multi-resolution geometric fusion. IEEE International Conference on 3D Digital Imaging and Modeling, Ottawa, May 12–15, pp. 181–188.

Horn, B.K.P., 1987. Closed-form solution of absolute orientation using unit quaternions. Journal of the Optical Society of America, A-4 (4), 629–642.

Horn, B.K.P., Hilden, H.M., Negahdaripour, S., 1988. Closed-form solution of absolute orientation using orthonormal matrices. Journal of the Optical Society of America, A-5 (7), 1128–1135.

Ikemoto, L., Gelfand, N., Levoy, M., 2003. A hierarchical method for aligning warped meshes. IEEE International Conference on 3D Digital Imaging and Modeling, Banff, October 6–10, pp. 434–441.

Jaw, J.J., 2000. Control surface in aerial triangulation. International Archives of Photogrammetry and Remote Sensing, 33 (B3), 444–451.

Johnson, A.E., Hebert, M., 1998. Surface matching for object recognition in complex three-dimensional scenes. Image and Vision Computing, 16 (9–10), 635–651.

Johnson, A.E., Hebert, M., 1999. Using spin images for efficient object recognition in cluttered 3D scenes. IEEE Transactions on Pattern Analysis and Machine Intelligence, 21 (5), 433–449.

Jokinen, O., Haggren, H., 1995. Relative orientation of two disparity maps in stereo vision. International Archives of Photogrammetry and Remote Sensing, 30 (5/W1), 157–162.

Jokinen, O., Haggren, H., 1998. Statistical analysis of two 3-D registration and modeling strategies. ISPRS Journal of Photogrammetry and Remote Sensing, 53 (6), 320–341.

Jost, T., Huegli, H., 2003. A multi-resolution ICP with heuristic closest point search for fast and robust 3D registration of range images. IEEE International Conference on 3D Digital Imaging and Modeling, Banff, October 6–10, pp. 427–433.

Karras, G.E., Petsa, E., 1993. DEM matching and detection of deformation in close-range photogrammetry without control. Photogrammetric Engineering and Remote Sensing, 59 (9), 1419–1424.

Kishon, E., Hastie, T., Wolfson, H., 1991. 3-D curve matching using splines. Journal of Robotic Systems, 8 (6), 723–743.

Krsek, P., Pajdla, T., Hlavac, V., 2002. Differential invariants as the base of triangulated surface registration. Computer Vision and Image Understanding, 87 (1–3), 27–38.

Lavallee, S., Szeliski, R., Brunie, L., 1991. Matching 3-D smooth surfaces with their 2-D projections using 3-D distance maps.

Proceedings of Geometric Methods in Computer Vision, San Diego, July 25–26, vol. 1570. SPIE, pp. 322–336.

Lucchese, L., Doretto, G., Cortelazzo, G.M., 2002. A frequency domain technique for range data registration. IEEE Transactions on Pattern Analysis and Machine Intelligence, 24 (11), 1468–1484.

Maas, H.G., 1994. A high-speed solid state camera system for the acquisition of flow tomography sequences for 3D least squares matching. International Archives of Photogrammetry and Remote Sensing, 30 (5), 241–249.

Maas, H.G., 2000. Least-Squares Matching with airborne laser scanning data in a TIN structure. International Archives of Photogrammetry and Remote Sensing, 33 (3A), 548–555.

Maas, H.G., Gruen, A., 1995. Digital photogrammetric techniques for high resolution three dimensional flow velocity measurements. Optical Engineering, 34 (7), 1970–1976.

Masuda, T., 2002. Registration and integration of multiple range images by matching signed distances fields for object shape modeling. Computer Vision and Image Understanding, 87 (1–3), 51–65.

Masuda, T., Yokoya, N., 1995. A robust method for registration and segmentation of multiple range images. Computer Vision and Image Understanding, 61 (3), 295–307.

Mitchell, H.L., Chadwick, R.G., 1999. Digital photogrammetric concepts applied to surface deformation studies. Geomatica, 53 (4), 405–414.

Murino, V., Ronchetti, L., Castellani, U., Fusiello, A., 2001. Reconstruction of complex environments by robust pre-aligned ICP. IEEE International Conference on 3D Digital Imaging and Modeling, Quebec, May 28–June 1, pp. 187–194.

Neugebauer, P.J., 1997. Reconstruction of real-world objects via simultaneous registration and robust combination of multiple range images. International Journal of Shape Modeling, 3 (1–2), 71–90.

Okatani, I.S., Deguchi, K., 2002. A method for fine registration of multiple view range images considering the measurement error properties. Computer Vision and Image Understanding, 87 (1–3), 66–77.

Pajdla, T., Van Gool, L., 1995. Matching of 3-D curves using semi-differential invariants. IEEE International Conference on Computer Vision, Cambridge, MA, June 20–23, pp. 390–395.

Park, S.Y., Subbarao, M., 2003. A fast point-to-tangent plane technique for multi-view registration. IEEE International Conference on 3D Digital Imaging and Modeling, Banff, October 6–10, pp. 276–283.

Parsi, B.K., Jones, J.L., Rosenfeld, A., 1991. Registration of multiple overlapping range images: scenes without distinctive features. IEEE Transactions on Pattern Analysis and Machine Intelligence, 13 (9), 857–871.

Pertl, A., 1984. Digital image correlation with the analytical plotter Planicomp C-100. International Archives of Photogrammetry and Remote Sensing, 25 (3B), 874–882.

Peters, G.J., 1974. Interactive computer graphics application of the parametric bi-cubic surface to engineering design problems. In: Barnhill, R., Riesenfeld, R. (Eds.), Computer Aided Geometric Design, Academic Press, pp. 259–302.

Pilgrim, L., 1996. Robust estimation applied to surface matching. ISPRS Journal of Photogrammetry and Remote Sensing, 51 (5), 243–257.

Postolov, Y., Krupnik, A., McIntosh, K., 1999. Registration of airborne laser data to surfaces generated by photogrammetric means. International Archives of Photogrammetry and Remote Sensing, 32 (3/W14), 95–99.

Potmesil, M., 1983. Generating models of solid objects by matching 3D surface segments. International Joint Conference on Artificial Intelligence, Karlsruhe, August 8–12, pp. 1089–1093.

Pottmann, H., Leopoldseder, S., Hofer, M., 2004. Registration without ICP. Computer Vision and Image Understanding, 95 (1), 54–71.

Pulli, K., 1999. Multiview registration for large data sets. IEEE International Conference on 3D Imaging and Modeling, Ottawa, October 4–8, pp. 160–168.

Pulli, K., Duchamp, T., Hoppe, H., McDonald, J., Shapiro, L., Stuetzle, W., 1997. Robust meshes from multiple range maps. IEEE International Conference on 3D Digital Imaging and Modeling, Ottawa, May 12–15, pp. 205–211.

Rogers, D.F., Adams, J.A., 1976. Mathematical Elements for Computer Graphics. McGraw-Hill Book Company, London, pp. 116–155.

Rosenholm, D., Torlegard, K., 1988. Three-dimensional absolute orientation of stereo models using digital elevation models. Photogrammetric Engineering and Remote Sensing, 54 (10), 1385–1389.

Roth, G., 1999. Registration two overlapping range images. IEEE International Conference on 3D Imaging and Modeling, Ottawa, October 4–8, pp. 191–200.

Rusinkiewicz, S., Levoy, M., 2001. Efficient variants of the ICP algorithm. IEEE International Conference on 3D Digital Imaging and Modelling, Quebec, May 28–June 1, pp. 145–152.

Sablatnig, R., Kampel, M., 2002. Model-based registration of front- and backviews of rotationally symmetric objects. Computer Vision and Image Understanding, 87 (1–3), 90–103.

Scaioni, M., Forlani, G., 2003. Independent model triangulation of terrestrial laser scanner data. International Archives of Photogrammetry, Remote Sensing and Spatial Information Sciences, 34 (5/W12), 308–313.

Schaffrin, B., Felus, Y.A., 2003. On total least-squares adjustment with constraints. Proceedings of IUGG General Assembly, Sapporo, Japan, June 30–July 11.

Schoenemann, P.H., 1966. A generalized solution of the Orthogonal Procrustes Problem. Psychometrika, 31 (1), 1–10.

Schoenemann, P.H., Carroll, R.M., 1970. Fitting one matrix to another under choice of a central dilation and a rigid motion. Psychometrika, 35 (2), 245–255.

Schwartz, J.T., Sharir, M., 1987. Identification of partially obscured objects in two and three dimensions by matching noisy characteristic curves. The International Journal of Robotics Research, 6 (2), 29–44.

Sequeira, V., Ng, K., Wolfart, E., Goncalves, J.G.M., Hogg, D., 1999. Automated reconstruction of 3D models from real environments. ISPRS Journal of Photogrammetry and Remote Sensing, 54 (1), 1–22.

Sharp, G.C., Lee, S.W., Wehe, D.K., 2002. ICP registration using invariant features. IEEE Transactions on Pattern Analysis and Machine Intelligence, 24 (1), 90–102.

Silva, L., Bellon, O.R.P., Boyer, K.L., Gotardo, P.F.U., 2003. Low-overlap range image registration for archaeological applications. IEEE Workshop on Applications of Computer Vision in Architecture, Madison, June 16–22, CD-ROM.

Soucy, G., Ferrie, F.P., 1997. Surface recovery from range images using curvature and motion consistency. Computer Vision and Image Understanding, 65 (1), 1–18.

Stamos, I., Leordeanu, M., 2003. Automated feature-based range registration of urban scenes of large scale. IEEE Computer Society Conference on Computer Vision and Pattern Recognition (CVPR), Madison, June 16–22, vol. II, pp. 555–561.

Szeliski, R., Lavallee, S., 1996. Matching 3-D anatomical surfaces with non-rigid deformations using octree-splines. International Journal of Computer Vision, 18 (2), 171–186.

Thirion, J.P., 1996. New feature points based on geometric invariants for 3D image registration. International Journal of Computer Vision, 18 (2), 121–137.

Turk, G., Levoy, M., 1994. Zippered polygon meshes from range images. In: Glassner, A. (Ed.), Proceedings of SIGGRAPH'94, Florida, July 24–29, pp. 311–318.

Vanden Wyngaerd, J., Van Gool, L., 2002. Automatic crude patch registration: towards automatic 3D model building. Computer Vision and Image Understanding, 87 (1–3), 8–26.

Vanden Wyngaerd, J., Van Gool, L., Koch, R., Proesmans, M., 1999. Invariant-based registration of surface patches. IEEE International Conference on Computer Vision, Kerkyra, September 20–27, pp. 301–306.

Wang, J.Y., Cohen, F.S., 1994. Part II: 3-D object recognition and shape estimation from image contours using B-splines, shape invariant matching, and neural networks. IEEE Transactions on Pattern Analysis and Machine Intelligence, 16 (1), 13–23.

Williams, J., Bennamoun, M., 2001. Simultaneous registration of multiple corresponding point sets. Computer Vision and Image Understanding, 81 (1), 117–142.

Williams, J.A., Bennamoun, M., Latham, S., 1999. Multiple view 3D registration: a review and a new technique. IEEE International Conference on Systems, Man, and Cybernetics, Tokyo, October 12–15, pp. 497–502.

Xu, Z., Li, Z., 2000. Least median of squares matching for automated detection of surface deformations. International Archives of Photogrammetry and Remote Sensing, 33 (B3), 1000–1007.

Yang, R., Allen, P., 1998. Registering, integrating, and building CAD models from range data. IEEE International Conference on Robotics and Automation, Leuven, May 16–20, pp. 3115–3120.

Zalmanson, G.H., Schenk, T., 2001. Indirect orientation of pushbroom sensors with 3-D free-form curves. Proceedings of Joint Workshop of ISPRS on High Resolution Mapping from Space, Hannover, September 19–21, CD-ROM.

Zhang, Z., 1994. Iterative point matching for registration of free-form curves and surfaces. International Journal of Computer Vision, 13 (2), 119–152.